Journal of Alloys and Compounds

MOF-derived synthesis of Co3O4 nanospheres with rich oxygen vacancies for long-term stable and highly selective n-butanol sensing performance

--Manuscript Draft--

Manuscript Number:	JALCOM-D-20-12174R1
Article Type:	Full Length Article
Keywords:	Co3O4 porous structure; metal-organic frameworks; oxygen vacancies; long-term stability; Gas sensing; n-butanol
Corresponding Author:	Lingli Cheng Shanghai University Shanghai, CHINA
First Author:	Lingli Cheng
Order of Authors:	Lingli Cheng
	Yongchao He
	Maozhi Gong
	Xinhua He
	Zhukai Ning
	Hongchuan Yu
	Zheng Jiao
Abstract:	Long-term stability and selectivity are crucial for the practical application of gas sensors, which are closely related to the microstructure and composition of sensor materials. In this work, Co-based metal organic framework (MOF) is used as a precursor and prepared by a simple hydrothermal method. After calcination, a series of Co3O4 nanospheres with various microstructures are derived. When the calcination temperature increases from 300℃ to 500℃, the microstructure of Co3O4 nanospheres changed from rough solid to porous, and then transformed into porous core-shell. When assembled into the gas sensors, the Co3O4 nanospheres with porous structure calcined at 400℃(Co3O4-400) show the highly selective response of 53.78 for 100 ppm n-butanol at the operating temperature of 140℃. Moreover, the theoretical limit of detection was calculated to be 150 ppb. The reproducibility, selectivity and stability of the gas sensor were further verified to be excellent. After 45 days, the response value of Co3O4-400 is at 86.74%, even after 75 days, the response value remains at 74.93%. The main reason can be attributed to the large specific surface area, abundant pore structure and a large number of oxygen vacancies on its surface. These findings provide reference for the development of p-type metal oxide semiconductor (MOS) sensors with long-term stability and high performance.
Order of Authors (with Contributor Roles):	Lingli Cheng
	Yongchao He
	Maozhi Gong
	Xinhua He
	Zhukai Ning
	Hongchuan Yu
	Zheng Jiao

Dear Editor:

We would like to submit the enclosed manuscript entitled "MOF-derived synthesis of Co_3O_4 nanospheres with rich oxygen vacancies for long-term stable and highly selective n-butanol sensing performance ", which we wish to be considered for publication in *Journal of Alloys and Compounds*.

In this work, the nano-spherical Co-MOF was chosen as a self-sacrificial template, which was synthesized by a simple solvothermal method. Then, by controlling the calcination temperature, a series of Co_3O_4 samples with different microstructure and composition have been prepared. Through the performance tests, the relationship between microstructure and performance has been verified. The Co_3O_4 nanospheres calcinated at 400℃(Co_3O_4-400) possess the best response sensitivity for n-butanol and long-term stability, which can be attributed to the porous and rich oxygen vacancies microstructure of it. Under the test temperature at 140℃, the response value of Co_3O_4-400 to 100 ppm n-butanol achieves 53.78, and the response value remains at 74.93% even after 75 days. Our work provides a facile MOF pyrolysis method for preparing long-term stable and high-performance gas sensitive MOS materials.

This paper is our original unpublished work and it has not been been published previously. All authors have seen the manuscript and approved to submit to your journal. If our manuscript can be accepted by *Journal of Alloys*

and Compounds, it will not be published elsewhere in the same form, in English or in any other language, without the written consent of the Publisher. Thank you very much for your attention and consideration.

Sincerely

Lingli Cheng

Prof. Dr

School of Environmental and Chemical Engineering, Shanghai University,

Shanghai 200444, China

Tel: (+86) 21 66136229, Fax: +86-21-6613-7787

E-mail: chenglingli@t.shu.edu.cn

The material prepared in our work has the following advantages:

Three kinds of Co_3O_4 nanospheres with different microstructure were prepared through MOF derivative method. The relationship between microstructure and gas sensing performance of materials has been clarified. The Co_3O_4 nanospheres calcinated at 400℃(Co_3O_4-400) possess the best response sensitivity for n-butanol and long-term stability, for its porous and rich oxygen vacancies microstructure.Under the test temperature at 140℃, the response value of Co_3O_4-400 to 100 ppm n-butanol achieves 53.78, and the response value remains at 74.93% even after 75 days.

Dear Editor,

We would like to send our response to reviewers of JALCOM-D-20-12174.

We are grateful for valuable comments and for careful and critical reading of this manuscript.

To reviewer 2:

We are grateful for valuable comments and for careful and critical reading of this manuscript. Our paper was much improved by helpful advices. We have revised our manuscript in line with the comments as follows.

1. As author has found that the order of % of oxygen vacancy in Co_3O_4 is Co_3O_4 400 (53.75%) > Co_3O_4 500 (35.76%) > Co_3O_4 300 (25.69%), why it is such in order? As we all know that Co(II) get oxidized into Co(III) when it thermally treated, hence it was expected that as the synthesis temperature was increased, the oxygen vacancy should decrease monotonously. However here the similar trend has not been followed.

Answer) Thanks for your valuable suggestion. You are right, generally, Co(II) get oxidized into Co(III) when it thermally treated, while the oxygen vacancy will decrease simultaneously. However, in our work, the XPS analysis results of Co_3O_4 samples (Fig. 1) show that the corresponding oxygen vacancy (O_V) contents of Co_3O_4-300, Co_3O_4-400 and Co_3O_4-500 are 25.69%, 53.75%, and 35.76%, respectively. To explain this, the TG and DTA analysis of Co-MOF precursor has been measured, as shown in Fig. 2. According to Fig. 2, the tricarboxylate linkers of Co-MOF precursors gradually decomposed in the temperature range of 150℃ to 300℃. At this stage, the decomposition rate of organic frames is relatively slow, so they mainly

react with the oxygen in air. And at the same time, the Co in the Co-MOF precursors also react with the oxygen in air to produce Co_3O_4. When the temperature goes from 300℃ to 450℃, the apparent mass loss is 48.8%, indicating the decomposition rate of organic frames is significantly accelerated. The higher decomposition rate results in the oxygen in air not meeting the decomposition of the organic framework, therefore the oxygen in Co_3O_4 participates in the reaction to produce oxygen vacancy on the surface of Co_3O_4. As we all know, Co_3O_4 can be regarded a compound formed by CoO and Co_2O_3. When the temperature increases to 500℃, the higher temperature results in the oxidation of Co(II) to Co(III). Hence the oxygen vacancy content of Co_3O_4-500 decreases.

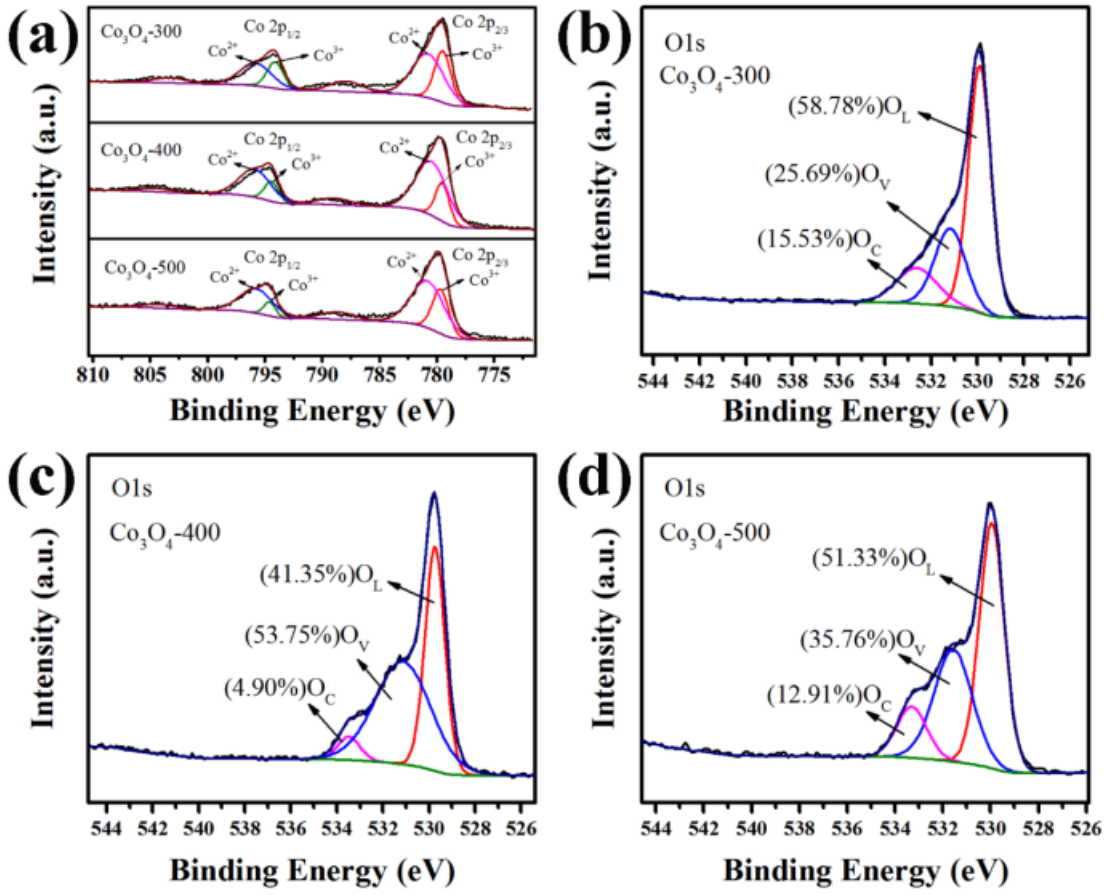

Fig. 1 (a) XPS spectra of Co 2p for porous Co_3O_4 samples; XPS spectra of O 1s and curve-fitting for (b) Co_3O_4-300, (c) Co_3O_4-400, (d) Co_3O_4-500.

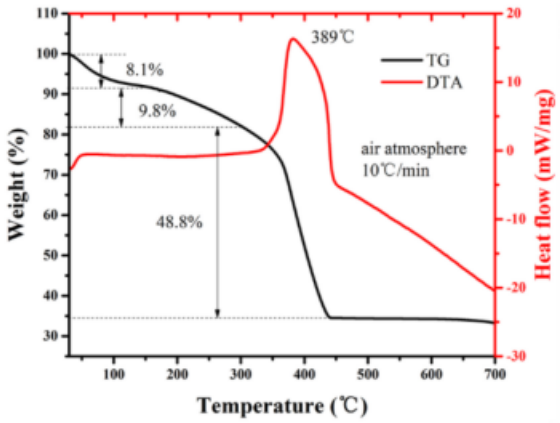

Fig. 2 TG and DTA analysis curves of the Co-MOF precursor

2. Author has provided the TG analysis of the MOF precursor, did author perform the TG of Co_3O_4 400, Co_3O_4 500, and Co_3O_4 300. I would suggest to do that in order to understand any carbonaceous materials present in the final Co_3O_4 structure.

Answer) Thanks for your valuable suggestion. With your suggestion, the TG analysis of Co_3O_4-300, Co_3O_4-400 and Co_3O_4-500 has been tested and the results are shown as Fig. 3. In Fig. 3, it is clear that the mass loss of the three samples is within 3.5%, indicating that the residual carbon content in all the samples is very low and the purity of samples is high.

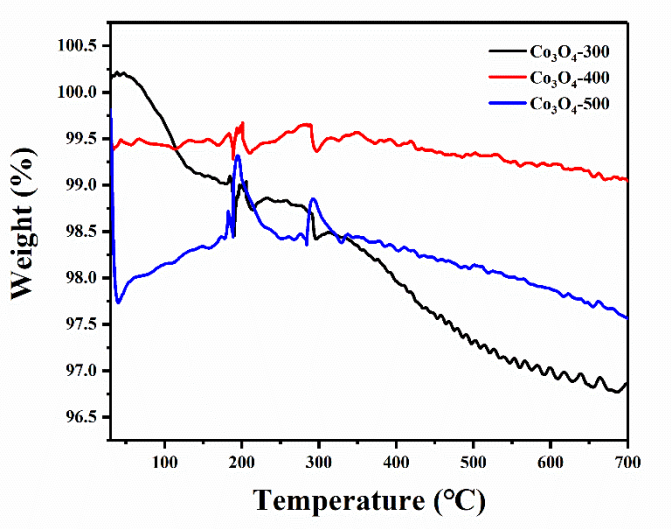

Fig. 3 TG analysis curves of Co_3O_4-300, Co_3O_4-400 and Co_3O_4-500

3. Add some of the recent Co_3O_4 based gas sensor in the introduction part.

i) Wen, Z.; Zhu, L.; Mei, W.; Hu, L.; Li, X.; Sun, L.; Cai, H.; Ye, Z. Rhombus-shaped Co_3O_4 nanorod arrays for high-performance gas sensor. Sens. Actuators, B 2013, 186, 172−179.

(ii) Mandal, S.; Rakibuddin, M.; Ananthakrishnan, R. Strategic Synthesis of SiO_2- Modified Porous Co_3O_4 Nano-Octahedra through the Nanocoordination Polymer Route for Enhanced and Selective Sensing of H_2 Gas over NO_x. ACS Omega 2018, 3, 648−661.

(iii) Choi, K.-I.; Kim, H.-R.; Kim, K.-M.; Liu, D.; Cao, G.; Lee, J.-H. C2H5OH sensing characteristics of various Co_3O_4 nanostructures prepared by solvothermal reaction. Sens. Actuators, B 2010, 146, 183−189.

Answer) Thanks for your valuable suggestion. With your suggestion, the above papers of recent Co_3O_4 based gas sensor have been added in the manuscript as the references [15], [21] and [24].

To reviewer 4:

We are grateful for valuable comments and for careful and critical reading of this manuscript. Our paper was much improved by helpful advises. We have revised our manuscript in line with the comments as follows.

1. Fig. 1 should be move to SI file.

Answer) Thanks for your valuable suggestion. Fig. 1 has been moved to SI file.

2. The response to NO_2 and SO_2 gases which are oxidizing gases should be evaluated.

Answer) Thanks for your valuable suggestion. The responses of the Co_3O_4-300, Co_3O_4-400 and Co_3O_4-500 samples to 100 ppm SO_2 and NO_2 were tested. As shown in Fig. 1, Co_3O_4-300, Co_3O_4-400 and Co_3O_4-500 sensors exhibit extremely low response to SO_2 and NO_2 at the optimal operating temperature as 140℃. It means all

Co_3O_4 sensors show the best selectivity to n-butanol among the examined gases at the operating temperature as140℃.

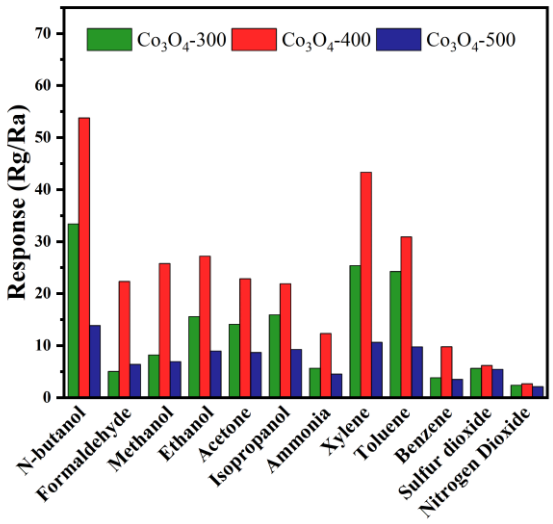

Fig. 1 Responses of Co_3O_4 samples to different gases at 140℃

3. Please statically calculate the LOD of sensor.

Answer) Thanks for your valuable suggestion. The LOD of Co_3O_4-300, Co_3O_4-400 and Co_3O_4-500 are calculated to be 215 ppb, 150 ppb and 190 ppb, respectively. The related content has been added in the revised paper, the specific description is as follows:

The theoretical detection limits for n-butanol in Co_3O_4 samples can be evaluated through linear extrapolation, the calculating of the LOD is LOD = 3 × (Standard Deviation/Slope）, which are calculated to be 215 ppb, 150 ppb, and 190 ppb, respectively.

4. BET surface areas as necessary to related the sensing properties to the surface area.

Answer) Thanks for your valuable suggestion. With the increment of calcination temperature, the specific surface area of Co_3O_4 samples decreased. The Co_3O_4-300 sample has the largest specific surface area of 69.8 m^2/g, while Co_3O_4-400 and Co_3O_4-300 are 39.3 m^2/g and 17.8 m^2/g, respectively. The pore size distribution calculated by the BJH method is shown in the inset of Fig. 1. The average pore

diameters of Co_3O_4-300 and Co_3O_4-400 are 10.5 nm and 23.6 nm, respectively. The pore sizes of Co_3O_4-500 are mainly distributed around 3.1 nm and 41.8 nm. The superior gas sensing performance of Co_3O_4-400 can be attributed to the large specific surface area, abundant pore structure and a large number of oxygen vacancies on its surface.

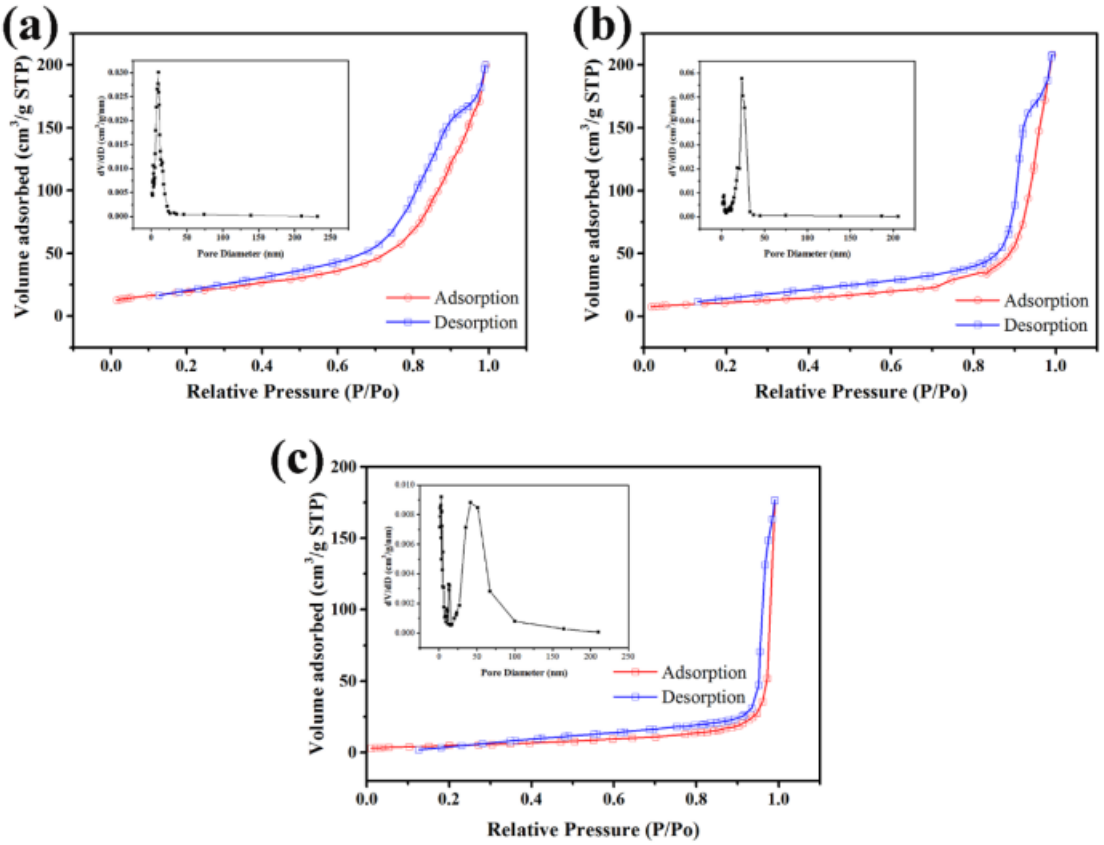

Fig. 2 Nitrogen adsorption-desorption isotherms and BJH pore size distribution plots (inset) of (a)Co_3O_4-300, (b)Co_3O_4-400, (c)Co_3O_4-500.

5. At 140 degree the dominant species are ionic oxygen ions rather than molecular oxygen ions. So equations should be modified.

Answer) Thanks for your valuable suggestion. You are right. According to the related reference, O^- is formed between 100℃and 300℃ [55]. The optimum operating temperature of the Co_3O_4 sensor in our work is 140℃, so the main oxygen species is O^- (Eq. (1)). We have modified equations and revised corresponding description in the revised manuscript.

$O_2 + 2e^- \rightarrow 2O^-$ Eq. (1)

[55] J. Guo, Y. Li, B. Jiang, H. Gao, G. Hao, Xylene gas sensing properties of hydrothermal synthesized SnO_2-Co_3O_4 microstructure, Sensors and Actuators B: Chemical, 310 (2020) 127780.

6. Why the gas sensor shows selectivity to buthanol among all other gases. This is very important issue.

Answer) Thanks for your valuable suggestion. According to your suggestion, the selectivity of Co_3O_4-400 to n-butanol has been analyzed in details. The reasons for the selectivity of Co_3O_4-400 to n-butanol include two points:

(i) The polarity of hydroxyl group (-OH) is stronger than amino group (-NH2), aldehyde (-CHO), carbonyl group (-C=O) and phenyl group. For containing hydroxyl group, the polarity of n-butanol is stronger than ammonia, formaldehyde, acetone, xylene, toluene and benzene. That means n-butanol has a very strong ability to provide electrons. And the large intrinsic crystal defects and rich oxygen vacancies of Co_3O_4-400 make it prefer to bound extra electrons as free carries, so it shows good selectivity to n-butanol. Furthermore, the excellent electron donor characteristics of n-butanol causes it react with the adsorbed oxygen species at the relatively low concentration, exhibiting relatively high response.

(ii) The diffusivity determines the residence time of the detected gas on the surface of gas sensor. And the longer residence time can improve the response of gas sensors to the detected gas. Comparing with ethanol and methanol, n-butanol has a lower diffusivity for its higher molecular weight. Hence, the residence time of n-butanol on Co_3O_4-400 is longer than other detected gases, which endows n-butanol higher response.

Once again, we like to express our heartfelt thanks to the editor and reviewers. We believe that our manuscript will be acceptable in this journal.

Sincerely yours,

Lingli Cheng

Prof. Dr.

School of Environmental and Chemical Engineering, Shanghai University,

Shanghai 200444, China

Tel: (+86) 21 66136229, Fax: +86-21-6613-6229

E-mail: chenglingli@shu.edu.cn

MOF-derived synthesis of Co_3O_4 nanospheres with rich oxygen vacancies for long-term stable and highly selective n-butanol sensing performance

Lingli Cheng[1,*], Maozhi Gong[1], Yongchao He[1], Xinhua He[1], Zhukai Ning[1], Hongchuan Yu[3], Zheng Jiao[2,*]

1. *School of Environmental and Chemical Engineering, Shanghai University, Shanghai, 200444, P.R. China*
2. *Shanghai Applied Radiation Institute, Shanghai University, Shanghai 201800, PR China*
3. *National Centre for Computer Animation (NCCA), Bournemouth University, BH125BB, UK*

---

* Corresponding author:

[1]Lingli Cheng, *Email:* chenglingli@t.shu.edu.cn, Tel./fax: +86 21 66136229.

[2]Zheng Jiao, *Email:* zjiao@shu.edu.cn, Tel./fax: +86 21 66135160.

Abstract

Long-term stability and selectivity are crucial for the practical application of gas sensors, which are closely related to the microstructure and composition of sensor materials. In this work, Co-based metal organic framework (MOF) is used as a precursor and prepared by a simple hydrothermal method. After calcination, a series of Co_3O_4 nanospheres with various microstructures are derived. When the calcination temperature increases from 300℃ to 500℃, the microstructure of Co_3O_4 nanospheres changed from rough solid to porous, and then transformed into porous core-shell. When assembled into the gas sensors, the Co_3O_4 nanospheres with porous structure calcined at 400℃(Co_3O_4-400) show the highly selective response of 53.78 for 100 ppm n-butanol at the operating temperature of 140℃. Moreover, the theoretical limit of detection was calculated to be 150 ppb. The reproducibility, selectivity and stability of the gas sensor were further verified to be excellent. After 45 days, the response value of Co_3O_4-400 is at 86.74%, even after 75 days, the response value remains at 74.93%. The main reason can be attributed to the large specific surface area, abundant pore structure and a large number of oxygen vacancies on its surface. These findings provide reference for the development of p-type metal oxide semiconductor (MOS) sensors with long-term stability and high performance.

Keywords: Co_3O_4 porous structure; metal–organic frameworks; oxygen vacancies; long-term stability; Gas sensing; n-butanol

1. Introduction

In recent years, with the strengthening of environmental remediation, volatile organic compounds (VOCs) has received more and more attention. VOCs, which widely exist in the modern society, refer to the organic compounds that exist at room temperature in the form of gas, including ethanol, acetone, n-butanol, et al [1]. Due to their volatile nature at room temperature, VOCs are potentially harmful to human health. Such as n-butanol, an important chemical raw material, is mainly used for the preparation of plasticizers, surfactants, butyl acrylate, butyl acetate and ethylene glycol butyl ether. It is also used as a solvent for coatings and as an extractant for biochemicals. N-butanol is an irritant and can cause damage to the respiratory system and the skin. When people are exposed in the n-butanol environment, they may feel drowsy and dizzy [2, 3]. Therefore, it is necessary to develop high performance n-butanol gas sensor for human health and industrial environment monitoring.

Metal oxide semiconductors (MOS) are the most promising gas sensing materials for detecting VOCs, due to their low cost, excellent reliability, high sensitivity and environmental friendliness [4-6]. Metal oxide semiconductors are classified into n-type and p-type, and most of the researchers are focused on the n-type MOS, such as ZnO [7], SnO_2 [8, 9], In_2O_3 [10], WO_3 [11]. Recently, p-type MOS with unique surface redox properties and good catalytic properties are being extensively studied. Co_3O_4 is a typical p-type metal oxide semiconductor with a unique AB_2O_4 spinel structure. The transformation between different valence states of Co^{2+}/Co^{3+} endows

with the excellent gas sensitive reactivity of Co_3O_4 materials [12-14]. However, p-type metal oxide semiconductors generally have some drawbacks, such as low sensitivity and long response/recovery time [15-17]. Researchers have used substantial methods to solve the problems, such as changing the morphology and structure of the materials [1, 18, 19], increasing their specific surface area and porosity [20, 21], doping [22, 23], loading [24, 25], forming composite materials [6, 26, 27], and so on.

Metal–organic frameworks (MOFs) are a new class of porous materials composed by metal ions and organic ligands [28]. Due to its various topologies, tunable structure and pore size, ultra-high specific surface area, unique morphology and other excellent properties, MOFs have received extensive attention from researchers. In terms of energy storage [29], adsorption [30], catalysis [31], gas sensing [6], drug delivery [32], etc., MOFs have great application prospects. In the field of gas sensing, MOFs can be used as self-sacrificing templates to prepare hollow, core-shell or porous nanostructures by controlling thermolysis conditions to improve the performance of gas sensors [16, 19]. Morphology of materials is the main factor on determining their performance. For instance, Zhang et al. [33] reported that ZIF-67 was used as a precursor template to synthesize the core shell, porous core shell and porous popcorn structure of Co_3O_4 by controlling the calcination environment, which significantly improved its response to acetone. The porous ZnO-Co_3O_4 hollow polyhedral structure synthesized by Xiong et al. [34] has a response value of 106 to 1000 ppm ethanol at 200℃. Shi et al. [27] synthesized hollow Co_3O_4/In_2O_3 microtubules derived from MOFs to significantly improve the sensing performance of triethylamine, and the

response to 50ppm TEA was 786.8. The above reports have demonstrated that metal oxides derived from MOFs generally have good morphology, large specific surface area, high porosity and more exposed active sites, which is benefit to improve the gas sensitivity of materials.

In this work, the nano-spherical Co-MOF was chosen as a self-sacrificial template, which was synthesized by a simple solvothermal method. Then, by controlling the calcination temperature, a series of Co_3O_4 samples with different microstructure and composition have been prepared. Through the performance tests, the relationship between microstructure and performance has been verified. The Co_3O_4 nanospheres calcinated at 400℃(Co_3O_4-400) possess the best response sensitivity for n-butanol and long-term stability, which can be attributed to the porous and rich oxygen vacancies microstructure of it. Under the test temperature at 140℃, the response value of Co_3O_4-400 to 100 ppm n-butanol achieves 53.78, and the response value remains at 74.93% even after 75 days. Therefore, our work provides a facile MOF pyrolysis method for preparing long-term stable and high-performance gas sensitive MOS materials.

2. Experimental section

2.1 Materials

Cobalt nitrate hexahydrate ($Co(NO_3)_2 \cdot 6H_2O$,≥99%), polyvinyl pyrrolidone (PVP, M.W.30,000) and N,N-dimethylformamide (DMF) were purchased from Sinopharm Chemical Reagent.1,3,5-benzenetricarboxylic acid (H_3BTC) was obtained from Tokyo Chemical Industry. All chemicals used in this study were of analytical grade and

without any further purification.

2.2 Synthesis of Co_3O_4 nanospheres

Typically, 3.000g PVP was dissolved into the 60 mL DMF to form a clear solution. In the synthesis process, PVP acts as a stabilizer, which is beneficial to the formation of the spherical structure Co-MOF [35]. Then, 0.300g H_3BTC, 1.048g $Co(NO_3)_2 \cdot 6H_2O$ were added to the above solution under magnetic stirring vigorously for 1 hour. After that, the mixed solution was transferred into a 100 ml Teflon-lined stainless steel autoclave, and placed into an oven with a constant temperature of 150℃ for 16 h. The obtained purple product was collected and purified by centrifugation, washed several times with DMF and ethanol, and then dried at 60℃ overnight. Finally, the as-prepared Co-MOF was annealed in a Tube furnace at 400℃ for 2 h with a heating rate of 2℃/min in air. And then, the porous structure Co_3O_4 nanospheres were successfully prepared. The complete synthesis process was simulated in Scheme. 1. The black Co_3O_4 powder obtained by calcination at three different temperatures (300℃, 400℃, 500℃)in air was labeled as Co_3O_4-300, Co_3O_4-400 and Co_3O_4-500, respectively.

<**Scheme 1**>

2.3 Characterization

The crystallographic structure of the prepared Co_3O_4 samples were determined by X-ray diffraction (XRD, Rigaku D/max-2200, Japan). The morphologies and microstructure were investigated by field-emission scanning electron microscope (FESEM, Hitachi, S-4800, Japan) and transmission electron microscope (TEM, JEOL,

200CX, Japan). More detailed structural and crystal features were characterized by selected-area electron diffraction (SAED) and high-resolution TEM (HRTEM, JEOL, 2100F, Japan). The chemical components of the samples were investigated by X-ray photoelectron spectroscopy (XPS, Thermo, ESCALAB 250Xl, USA). The N_2 adsorption–desorption isotherms were measured on an automatic surface analyzer (Quantachrome, Quadrasord SI, USA). The surface area and the pore size distribution were evaluated using Brunauer–Emmett–Teller (BET) and Barrett–Joyner–Halenda (BJH) methods, respectively. The thermal decomposition behavior of the MOF precursor was studied by thermogravimetric analyzer (TGA, Mettler Toledo, TGA/DSC 3+, Switzerland).

2.4 Fabrication and measurements of gas sensors

The Co_3O_4 samples obtained by calcination at different temperatures were mixed with an appropriate amount of ethanol and ground to form a uniform paste. Then, the paste was applied to the surface of a hollow Al_2O_3 ceramic tube. The sample completely covered the area between the two gold electrodes on the surface of the ceramic tube. Subsequently, the ceramic tube coated with the sample was placed in an oven and dried at 60 ° C for 2 hours. Next, a Ni-Cr alloy heating wire was inserted into the ceramic tube, and the operating temperature was changed by adjusting the heating voltage. Finally, the heating wire and the two pairs of Pt wires on the ceramic tube gold electrode were welded to the sensor base to form a complete sensor device, as shown in Fig.1. The sensing performance of the material was tested using the WS-30A gas sensor test system (Winsen Electronics Co., Ltd., Henan, China) as

shown in Fig.1S. Before the test, the sensor was aged at 300 ° C for 2 days on an aging device to improve the stability of its sensing performance. The gas response (sensitivity) is defined as $S=R_g/R_a$, where R_g is the resistance of the sensor in the target gas and R_a is the resistance in ambient air. The response of the sensor is the relative change in resistance of the material in the air and in the target gas [15]. The response and recovery times are defined as the time required for the sensor to reach 90% of the total resistance change during the process of adsorbing and desorbing the target gas, respectively [36].

< **Fig. 1**>

3. Results and discussion

3.1. Structural and morphological characteristics

The Co-MOF was used as the precursor, and a series of Co_3O_4 nanospheres were synthesized by calcinating at different temperature. The XRD pattern of Co-MOF is shown in Fig. S2, revealing that the Co-MOF precursor is a crystalline material, which is consistent with the results reported by previous researchers [37, 38]. Subsequently, the morphological and structural changes of Co-MOF-derived metal oxide Co_3O_4 at different calcination temperatures were investigated.

< **Fig. 2**>

The corresponding powder X-ray diffraction (XRD) patterns of the calcined products can provide information on the crystallinity and phase composition, as shown in Fig. 2. The XRD patterns of the three samples all have identical diffraction peak positions and similar peak shapes, which are in good agreement with the cubic

spinel structure of Co_3O_4 (JCPDS no. 043-1003), indicating that the Co-MOF had been successfully converted into Co_3O_4. The diffraction lines are located at 2θ =19.0, 31.3, 36.8, 44.8, 59.4, 65.2° marked by their index's planes ((1 1 1), (2 2 0), (3 1 1), (4 0 0), (5 1 1), (4 4 0)), respectively. No other impurity peaks were detected, indicating that the Co_3O_4 samples are of high purity, and the strong peaks and spikes of the samples also confirm the high crystallinity. The change of the calcination temperature only changed the crystallinity of the products, but had no effect on the composition. Among the three kinds of Co_3O_4 samples, Co_3O_4-500 has the best crystallinity and the strongest diffraction peak intensity followed by Co_3O_4-400. And Co_3O_4-300 has the lowest crystallinity.

< **Fig. 3**>

The morphologies of the precursor and products were characterized by field emission scanning microscopy, as shown in Fig. 3. Fig. 3(a) shows that the synthesized Co-MOF is about 600 nm-900 nm in diameter, and the particles formed are relatively uniform. As observed in Fig. 3(b), the as-prepared Co-MOF precursor has a regular spherical structure and the surface is slightly rough. Fig. 3(c-h) exhibits the FESEM image of Co_3O_4 samples at different calcination temperatures. For the calcined sample at 300℃, Fig. 3 (c, d) show the spherical structure similar to that of the Co-MOF precursor, and the morphology remained intact. As observed from the inset in Fig. 3(d), the Co_3O_4-300 sample has a rougher surface than the precursor, which was mainly caused by thermal decomposition of the organic ligand. When the calcination temperature was raised to 400℃, Co_3O_4-400 still maintained a complete

spherical shape, as shown in Fig.3 (e, f). It can be seen from Fig. 3(f) and its inset that the surface roughness of the Co_3O_4 sample is further increased, and the particle size is gradually reduced to a diameter of about 500 nm. At the same time, the framework structure exhibits a complete sphere composed of ~25nm tiny nanoparticles, and the pore diameter is further increased. When the calcination temperature was 500℃, the Co_3O_4-500 sample produced ~50nm nanoparticles during the formation process, and significant large pores can be seen between the tiny nanoparticles, as shown in Fig. 3 (g, h). Compared to Co_3O_4-400, the nanoparticles constituting the Co_3O_4-500 sample are larger in size, resulting in an increase in pores between the particles. The calcination temperature was increased from 300℃ to 500℃, the Co_3O_4 products were able to maintain a complete spherical morphology, but the surface became rougher and the pores became larger.

< **Fig. 4**>

In order to further study the microstructure changes of Co_3O_4 products affected by calcination temperature, TEM and HRTEM were used to characterize the samples. In Fig. 4(a), the internal structure of the Co_3O_4-300 sample is in a solid state, and no obvious porous structure can be observed. Fig. 4(b) shows that a large number of pores can be identified on the surface of Co_3O_4-400, and the porous nanospheres were successfully prepared. When the calcination temperature was raised to 500℃, the porous structure gradually transformed into the core-shell structure and the internal pore size increased, as shown in Fig. 4(c). When the calcination temperature increased from 300℃ to 500℃, the structure of the products changed from the rough solid

structure to the porous structure, and then further transformed into the porous core-shell structure. The formation of a large number of pores in the products are due to the organic ligands being oxidized to CO_2 and H_2O and volatilized into the air. Moreover, it can be seen from the HRTEM in Fig. 4(d) that the lattice fringes of the Co_3O_4-400 sample is 2.86 Å, which corresponds to the (220) crystal planes of spinel Co_3O_4. The selected area electronic diffraction (SAED) pattern (inset image of Fig. 4(d)) exhibits several concentric rings, indicating that the Co_3O_4-400 spherical nanostructure is polycrystalline in nature and has good crystallinity.

In addition, the thermal decomposition behavior of the Co-MOF precursor was first studied by thermogravimetric analysis (TG) and differential thermal analysis (DTA), as shown in Fig.S3. Below 150℃, the mass loss is about 8.1%, mainly to remove adsorbed water molecules, gases and solvents. The tricarboxylate linkers gradually decomposed in the temperature range of 150℃ to 300℃. From 300℃ to 450℃, the apparent mass loss is 48.8%, indicating that the organic ligands decomposed and the metal-organic frameworks were completely converted into the metal oxides. Such a significant mass reduction means that a large amount of gas (CO_2, H_2O) was produced in the process of decomposing the organic matter [39-41]. According to the DTA analysis, the corresponding exothermic peak appeared at 389℃. When the pyrolysis temperature exceeded 450℃, the sample quality remained substantially stable.

Nitrogen adsorption-desorption isotherms were conducted in order to identify the specific surface areas and porosity structure of as-synthesized Co_3O_4 nanospheres, and the results are shown in Fig. S4. The N_2 adsorption-desorption curves of all products

show typical IV isotherms with H3 hysteresis loop, indicating the presence of the mesoporous structure. The specific surface area of the product decreases as the calcination temperature increases. The Co_3O_4-300 sample has the largest specific surface area of 69.8 m^2/g, and Co_3O_4-400 and Co_3O_4-500 are 39.3 m^2/g and 17.8 m^2/g, respectively. The pore size distribution calculated by the BJH method is shown in the inset of Figure S4 . The average pore diameters of Co_3O_4-300 and Co_3O_4-400 are 10.5 nm and 23.6 nm, respectively, and the pore sizes of Co_3O_4-500 are mainly distributed at 3.1 nm and 41.8 nm. As the calcination temperature increases, the pore size of the Co_3O_4 product increases, which is consistent with the results observed in the SEM. The results of various characterizations show that the calcination temperature has a significant effect on the structure and morphology of Co_3O_4 nanospheres formed by self-assembly of nanoparticles, especially with MOF as a self-sacrificing template.

3.2. Gas sensing properties

< **Fig. 5**>

The gas sensing performance of as prepared Co_3O_4 samples were evaluated through testing the working temperature, response value, response/recovery time, stability and selectivity. The working temperature is an important indicator to measure the performance of gas sensors, which is of great significance for the practical application of sensors. Fig. 5 depicts the response of three Co_3O_4 samples to 100 ppm n-butanol over a range of 100℃-220℃. From 100℃ to 140℃, the response of these three sensors increases with the increment of operating temperature until the maximum response at 140℃ is obtained. The Co_3O_4-400 sample exhibits the highest response

of 53.78 for 100 ppm n-butanol at 140℃, comparing with 33.40 for Co_3O_4-300, and 13.86 for Co_3O_4-500. Subsequently, when the operating temperature increases, the response decreases gradually. This phenomenon can be attributed to the following reasons [12]. At first, when the operating temperature is relatively low, most target gas is inactive, as well as there is not enough activation energy to react with the surface-adsorbed oxygen species, which leads to a low response. As the temperature increases, the gas molecules obtain enough energy to overcome the activation energy barrier, so the response enhances. Then, when the temperature exceeds the optimum reaction temperature, the desorption rate of the gas molecules on the surface of sensing materials is greater than the corresponding adsorption rate, which causes the response value diminish greatly. Therefore, the sensor exhibits the response characteristics of "increase-maximum-decrease" [42]. The optimal operating temperature can be determined to be 140℃, which is critical for subsequent gas-sensitive performance tests.

< **Fig. 6**>

The transient sensing curves of the three sensors for 100ppm n-butanol at the optimum operating temperature are shown in Fig. 6(a). All the sensors show similar response and recovery processes. Fast response and recovery processes are very important for the practical application of gas sensors. The response and recovery time are calculated and labeled in Fig. 6(b, c, d). The response times of Co_3O_4-300, Co_3O_4-400, and Co_3O_4-500 are 152s, 99s, and 153s, respectively, and the recovery times are 37s, 50s, and 53s, respectively. Comparing with Co_3O_4-300 and Co_3O_4-500,

Co_3O_4-400 has a much shorter response time, but its recovery time is slightly longer than that of Co_3O_4-300.

< **Fig. 7**>

Fig. 7 (a) is the typical dynamic sensing transient curves of Co_3O_4 sensors at different n-butanol concentrations (3ppm-100ppm). All the sensors showed good response, and the response value enhanced with the increment of n-butanol concentration. The relationship of response values and n-butanol concentrations for three samples are displayed in Fig. 7(b). When the concentration of n-butanol is 3ppm, the response of Co_3O_4-300, Co_3O_4-400 and Co_3O_4-500 are 1.87, 8.74 and 1.94, respectively. It is obvious that Co_3O_4-400 has the lowest detection limit in the three sensors. Meanwhile, the Co_3O_4-400 exhibits the highest response value at each n-butanol concentration. It can also be observed in Fig. 7(b) that the response value of the Co_3O_4-400 sample increases significantly in the concentration range from 3 ppm to 20 ppm, and then it gets saturated. The linear relationship between n-butanol concentration and the response values in the range from 3 ppm to 20 ppm is shown in Fig. 7(c). The theoretical detection limits for n-butanol in Co_3O_4 samples can be evaluated through linear extrapolation, which are calculated to be 215 ppb, 150 ppb, and 190 ppb, respectively [43]. The above results indicate that the Co_3O_4-400 sample owns excellent sensitivity for n-butanol, which means that it has great application potential in low concentration n-butanol sensing.

Stability (repeatability) is crucial for a sensor in the commercial application. To test the stability of Co_3O_4 sensors, they were measured over 6 periods (a period means a

complete cycle of response and recovery procedures to 100 ppm n-butanol). The sensing transient curves are shown in Fig. 7(d). During 6 periods, the instantaneous response values of the sensors have no obvious change, which proves the good reversibility and repeatability of the Co_3O_4 sensors prepared in our work.

Selectivity is another important factor for the practical application of gas sensors. The response of all Co_3O_4 samples toward 100 ppm VOCs mixture (including n-butanol, formaldehyde, methanol, ethanol, acetone, isopropanol, ammonia, xylene, toluene and benzene) is shown in Fig. 7(e). The Co_3O_4-400 sample not only shows the highest response to all the VOCs, but also exhibits the best selectivity to n-butanol. The response value of Co_3O_4-400 to n-butanol is 1.3-5.5 times than other VOCs. Among them, only xylene could make interference with n-butanol, which may be due to similar optimal operating temperature and chemical reactivity energy.

Long-term stability as a significant impact on the durability of sensors has been tested. In order to evaluate the influence of the external environment on the stability of the gas sensor, the Co_3O_4-400 sensor was placed in the air for 45 days. After 45 days, the response value of Co_3O_4-400 to n-butanol still can achieve 46.65, which was 86.74% of the initial value, and show good response-recovery performance, indicating that the stability of Co_3O_4-400 is splendid. Then, the response of the Co_3O_4-400 to 100 ppm n-butanol at 140℃ was continuously tested for 30 days，as shown in Fig.7(f). Within 30 days, the response of the Co_3O_4-400 sensor fluctuated slightly. After the 75 days' test, the response value of the Co_3O_4-400 is tested to be 40.30, retaining 74.93% without significant reduction, further indicating that it has good

long-term stability and guarantees its service life. Furthermore, the Co_3O_4-400 sensor synthesized in this work is compared with the reported Co_3O_4 sensors. The results are listed in Table 1. It can be seen from this, the gas sensor prepared in this work can effectively enhance the response of n-butanol and reduce the operating temperature. Considering the response and the optimal operating temperature, the unique 3D porous structure Co_3O_4 nanospheres gas sensor shows superior gas sensing properties and has great practical application potential.

< **Table 1**>

3.3. Gas sensing mechanism

< **Fig. 8**>

The reaction process of the target gas on the surface of the material plays an important role in the sensing process. In order to further study the electronic states of the surface elements, the XPS analysis of Co_3O_4 samples was performed. Fig. 8(a) shows the high-resolution spectrum of Co 2p, in which there are two characteristic peaks and two satellite peaks. Both the positions and distributions of the Co 2p XPS peaks in all the Co_3O_4 samples are similar. Two characteristic peaks at 779.8 eV and 794.9 eV belong to the Co $2p_{3/2}$ and Co $2p_{1/2}$ spin-orbital peaks of Co_3O_4, respectively, and their corresponding satellite peaks are at 789.7 eV and 804.6 eV. The difference between Co^{2+} and Co^{3+} peaks can be observed after curve-fitting, as shown in Fig. 8(a). Fig. 8 (b-d) show the high resolution XPS spectra of O1s for Co_3O_4 samples. These spectra can be divided into three fitted peaks, corresponding to O_L, O_V and O_C, respectively. O_L refers to the lattice oxygen species, which contributes little to the gas

response for its stability. O_V means that there are oxygen vacancies on the surface of samples, which can provide active sites for the gas adsorption and reaction on the surface of sensing materials. O_C represents the chemically adsorbed oxygen species, such as O_2^-, O^-, O^{2-}. When the calcination temperature is 300℃, 400℃, and 500℃, the corresponding O_V contents are 25.69%, 53.75%, and 35.76%, respectively. Obviously, Co_3O_4-400 has the highest oxygen vacancy content, which leads to its highest response to 100 ppm n-butanol at 140℃. Heat treatment is one of the common methods for the controllable defect generation of nanomaterials, and it can be adjusted by controlling the calcination temperature and the atmosphere. The defects due to heat treatment are mainly the result of the release and recovery of O atoms in the material lattice. Therefore, in the presence of oxygen, the oxygen vacancy concentration will have a high point [50]. The presence of surface oxygen vacancies plays a crucial role in chemical sensing. Positively charged oxygen vacancies tend to trap electrons, effectively separating electron-hole pairs and improving sensing performance. The oxygen vacancy content of Co_3O_4-300 is 25.69 %, which is lower than 35.76 % of Co_3O_4-500, but Co_3O_4-300 has higher response to 100ppm n-butanol. This may be due to the fact that the specific surface area of Co_3O_4-300 is much larger than that of Co_3O_4-500.

The other major factor affecting gas sensing performance is specific surface area and pore size. In general, a large specific surface area enables the sensing material to adsorb more oxygen species. The Co_3O_4-400 sample has a specific surface area of 39.3 m^2/g. Meanwhile, the porous structure of Co_3O_4-400 provides a large amount of

exposed area for gas sensing, which is conducive to improving its sensing performance of n-butanol. According to surveys, the average pore size of many metal oxide sensing materials is around 25 nm [8, 22, 45, 47]. The unique porous structure of the product and the appropriate pore size facilitate the penetration of gas molecules into the interior of the sensing material. This allows the hole accumulation layer to be formed on both the outer layer and the inner layer of the materials, resulting in a low initial resistance in the air.

Furthermore, the good catalytic activity of Co_3O_4 also plays a positive role in improving gas sensitivity, in which Co^{3+} is capable of oxidizing reductive gases [26]. During the catalytic process, the reductive gas reacts with oxygen ions adsorbed on the Co^{3+} active site, causing a change in resistance and generating Co^{2+}. Then Co^{2+} can be oxidized to active Co^{3+} by the gaseous oxygen molecule in the air. In the target gas, Co^{3+} in Co_3O_4 can promote the oxidation reaction of n-butanol, improving the sensing performance. In summary, the excellent gas sensing performance of the Co_3O_4-400 material for n-butanol can be attributed to the following three factors: (i) abundant oxygen vacancies; (ii) the unique porous structure with a large specific surface area; (iii) Catalytic activity of Co_3O_4 for n-butanol.

< **Fig. 9**>

The sensing characteristics of MOS-based gas sensors are affected by the surface reaction of the sensor layer. The sensing mechanism of p-type semiconductor oxide Co_3O_4 is closely related to the change of resistance. However, the change in resistance is mainly due to the change in the concentration of holes in the surface region [51]. As

shown in Fig. 9, when the Co_3O_4 sensor is exposed to the air, oxygen molecules are adsorbed on the surface of Co_3O_4, and electrons (e^-) are trapped from the conduction band to form different oxygen species (such as O_2^-, O^-, O^{2-}). When the temperature is lower than 150 ° C, the main oxygen species is O_2^-. O^- is formed between 150℃and 400℃, and O^{2-} is formed above 400℃ [14, 52]. The optimum operating temperature of the Co_3O_4 sensor in this work is 140℃, so the main oxygen species is O_2^- (Eq. (1)). With the changing of adsorbed oxygen species, the electron depletion layer of Co_3O_4 is generated and the hole concentration is increased to form the hole accumulation layer [53]. Since the majority carrier of Co_3O_4 is hole, the resistance of Co_3O_4 in the air is low. When the n-butanol gas is injected, the adsorbed oxygen species (O_2^-) react with the reductive n-butanol (Eq. (2)). The electrons generated in this process return to the conduction band of Co_3O_4, causing the electron-hole pairs recombine, the hole accumulation layer shrink, and the resistance of materials increase. The recovery process is just the reversible process of the above reaction. When the n-butanol gas is removed, the oxygen molecules again capture electrons from the conduction band, reducing the resistance to its initial value.

$$O_2 + e^- \rightarrow O_2^- \qquad \text{Eq. (1)}$$

$$CH_3(CH_2)_3OH + 6O_2^- \rightarrow 4CO_2 + 5H_2O + 6e^- \qquad \text{Eq. (2)}$$

4. Conclusion

The porous structure Co_3O_4 was successfully prepared by the precursor derivatization strategy of metal-organic framework and applied to gas sensing.

Through performance test, the Co_3O_4-400 exhibits the best gas sensitivity. At the optimum testing temperature, the response to 100 ppm n-butanol is 53.78 and the theoretical limit of detection is 150 ppb. Co_3O_4-400 also owns good stability and reproducibility. After six consecutive cycles of testing, there was no significant change in the response curve to n-butanol. After left in the air for 45 days, the response value of Co_3O_4-400 to n-butanol was tested to be 46.65, which was 86.74% of the initial value. Even in the following 30-day long-term test, the response value was still stable, retaining 74.93% of the initial value. The unique spherical porous microstructure make Co_3O_4-400 have a large specific surface area and a suitable pore size. The larger specific surface area can adsorb a large amount of gas, and the proper pore size is conducive to the diffusion of gas molecules into the sensing material, thereby helping to improve the gas sensing performance. Additionally, the abundant oxygen vacancies generated by the heat treatment provide a large number of active sites and also help to improve the sensing performance. Our work provides a strategy for developing p-type semiconductor metal oxide sensors with high response, low detection limit and low temperature.

Acknowledgements

This work was supported by the National Natural Science Foundation of China (No. 21671128, 21671130).

Appendix A. Supporting Information

Figures showing: (S1) Digital photograph of the gas sensor test system. (S2) XRD pattern of Co-MOF. (S3) TG and DTA analysis curves of the Co-MOF precursor. (S4)

Nitrogen adsorption-desorption isotherms and BJH pore size distribution plots (inset) of (a)Co_3O_4-300, (b)Co_3O_4-400, (c)Co_3O_4-500.

References:

[1] M. Wang, Z. Shen, X. Zhao, F. Duanmu, H. Yu, H. Ji, Rational shape control of porous Co_3O_4 assemblies derived from MOF and their structural effects on n-butanol sensing, Journal of hazardous materials, 371 (2019) 352-361.

[2] A. Mirzaei, S.G. Leonardi, G. Neri, Detection of hazardous volatile organic compounds (VOCs) by metal oxide nanostructures-based gas sensors: A review, Ceramics International, 42 (2016) 15119-15141.

[3] M. Wang, T. Hou, Z. Shen, X. Zhao, H. Ji, MOF-derived Fe_2O_3: Phase control and effects of phase composition on gas sensing performance, Sensors and Actuators B: Chemical, 292 (2019) 171-179.

[4] M. Wang, T. Hou, X. Zhao, H. Yu, H. Ji, Crucial structural effects of porous Co_3O_4 derived from Prussian blue analogue on the enhanced gas sensing performance, Materials Letters, 242 (2019) 83-86.

[5] D. Zhang, Z. Yang, Z. Wu, G. Dong, Metal-organic frameworks-derived hollow zinc oxide/cobalt oxide nanoheterostructure for highly sensitive acetone sensing, Sensors and Actuators B: Chemical, 283 (2019) 42-51.

[6] F. Qu, T. Thomas, B. Zhang, X. Zhou, S. Zhang, S. Ruan, M. Yang, Self-sacrificing templated formation of $Co_3O_4/ZnCo_2O_4$ composite hollow nanostructures for highly sensitive detecting acetone vapor, Sensors and Actuators B: Chemical, 273 (2018) 1202-1210.

[7] T. Zou, R. Zhao, Z. Wang, R. Zhao, Z. Wang, Y. Yang, X. Xing, Y. Wang, Sensitive and selective n-butanol gas detection based on ZnO nanocrystalline synthesized by a low-temperature solvothermal method, Physica E: Low-dimensional Systems and Nanostructures, 103 (2018) 143-150.

[8] Y. Wang, Y. Zeng, L. Wang, Z. Lou, L. Qiao, H. Tian, W. Zheng, Ultrathin nanorod-assembled SnO_2 hollow cubes for high sensitive n-butanol detection, Sensors and Actuators B: Chemical, 283 (2019) 693-704.

[9] R. Zhao, Z. Wang, Y. Yang, X. Xing, T. Zou, Z. Wang, Y. Wang, Raspberry-like SnO_2 hollow nanostructure as a high response sensing material of gas sensor toward n-butanol gas, Journal of Physics and Chemistry of Solids, 120 (2018) 173-182.

[10] J. Wang, Z. Zheng, D. An, X. Tong, Q. Zhou, Highly selective n-butanol gas sensor based on porous In_2O_3 nanoparticles prepared by solvothermal treatment, Materials Science in Semiconductor Processing, 83 (2018) 139-143.

[11] Y. Wang, B. Zhang, J. Liu, Q. Yang, X. Cui, Y. Gao, X. Chuai, F. Liu, P. Sun, X. Liang, Y. Sun, G. Lu, Au-loaded mesoporous WO_3 : Preparation and n-butanol sensing performances, Sensors and Actuators B: Chemical, 236 (2016) 67-76.

[12] D. Han, Y. Ji, F. Gu, Z. Wang, Cobalt oxide nanorods with special pore structure for enhanced ethanol sensing performance, Journal of colloid and interface science, 531 (2018) 320-330.

[13] B. Zhang, X. Zhou, C. Jiang, F. Qu, M. Yang, Facile synthesis of mesoporous Co_3O_4 nanofans as gas sensing materials for selective detection of xylene vapor,

Materials Letters, 218 (2018) 127-130.

[14] X. Zhang, J. Wang, L. Xuan, Z. Zhu, Q. Pan, K. Shi, G. Zhang, Novel Co_3O_4 nanocrystalline chain material as a high performance gas sensor at room temperature, Journal of Alloys and Compounds, 768 (2018) 190-197.

[15] L. Li, M. Liu, S. He, W. Chen, Freestanding 3D mesoporous Co_3O_4@carbon foam nanostructures for ethanol gas sensing, Analytical chemistry, 86 (2014) 7996-8002.

[16] Y. Lu, W. Zhan, Y. He, Y. Wang, X. Kong, Q. Kuang, Z. Xie, L. Zheng, MOF-templated synthesis of porous Co_3O4 concave nanocubes with high specific surface area and their gas sensing properties, ACS applied materials & interfaces, 6 (2014) 4186-4195.

[17] T. Zhou, T. Zhang, J. Deng, R. Zhang, Z. Lou, L. Wang, P-type Co_3O_4 nanomaterials-based gas sensor: Preparation and acetone sensing performance, Sensors and Actuators B: Chemical, 242 (2017) 369-377

[18] X. Dong, Y. Su, T. Lu, L. Zhang, L. Wu, Y. Lv, MOFs-derived dodecahedra porous Co_3O_4: An efficient cataluminescence sensing material for H_2S, Sensors and Actuators B: Chemical, 258 (2018) 349-357.

[19] Y.M. Jo, T.H. Kim, C.S. Lee, K. Lim, C.W. Na, F. Abdel-Hady, A.A. Wazzan, J.H. Lee, Metal-organic framework-derived hollow hierarchical Co_3O_4 nanocages with tunable size and morphology: ultrasensitive and highly selective detection of methylbenzenes, ACS applied materials & interfaces, 10 (2018) 8860-8868.

[20] J. Tan, M. Dun, L. Li, X. Huang, Co_3O_4 nanoboxes with abundant porestructure boosted ultrasensitive toluene gas sensors, Materials Research Express, 5 (2018) 045036.

[21] R. Jiang, L. Jia, X. Guo, Z. Zhao, J. Du, X. Wang, P. Wang, F. Xing, Dimethyl sulfoxide-assisted hydrothermal synthesis of Co_3O_4-based nanorods for selective and sensitive diethyl ether sensing, Sensors and Actuators B: Chemical, 290 (2019) 275-284.

[22] L. Guo, F. Chen, N. Xie, C. Wang, X. Kou, Y. Sun, J. Ma, X. Liang, Y. Gao, G. Lu, Metal-organic frameworks derived tin-doped cobalt oxide yolk-shell nanostructures and their gas sensing properties, Journal of colloid and interface science, 528 (2018) 53-62.

[23] J. Wu, Y. Yang, C. Zhang, H. Yu, L. Huang, X. Dong, J. Wang, X. Wang, Extremely sensitive and accurate H_2S sensor at room temperature fabricated with In-doped Co_3O_4 porous nanosheets, Dalton transactions, 48 (2019) 7720-7727.

[24] W.T. Koo, S. Yu, S.J. Choi, J.S. Jang, J.Y. Cheong, I.D. Kim, Nanoscale PdO Catalyst Functionalized Co3O4 Hollow Nanocages Using MOF Templates for Selective Detection of Acetone Molecules in Exhaled Breath, ACS applied materials & interfaces, 9 (2017) 8201-8210.

[25] S.J. Hwang, K.I. Choi, J.W. Yoon, Y.C. Kang, J.H. Lee, Pure and palladium-loaded Co_3O_4 hollow hierarchical nanostructures with giant and ultraselective chemiresistivity to xylene and toluene, Chemistry, 21 (2015)

5872-5878.

[26] J. Xiao, K. Diao, Z. Zheng, X. Cui, MOF-derived porous ZnO/Co_3O_4 nanocomposites for high performance acetone gas sensing, Journal of Materials Science: Materials in Electronics, 29 (2018) 8535-8546.

[27] S. Shi, F. Zhang, H. Lin, Q. Wang, E. Shi, F. Qu, Enhanced triethylamine-sensing properties of P-N heterojunction Co_3O_4/In_2O_3 hollow microtubes derived from metal–organic frameworks, Sensors and Actuators B: Chemical, 262 (2018) 739-749.

[28] B. Li, J. Liu, Q. Liu, R. Chen, H. Zhang, J. Yu, D. Song, J. Li, M. Zhang, J. Wang, Core-shell structure of ZnO/Co_3O_4 composites derived from bimetallic-organic frameworks with superior sensing performance for ethanol gas, Applied Surface Science, 475 (2019) 700-709.

[29] S. Gao, Y. Sui, F. Wei, J. Qi, Q. Meng, Y. Ren, Y. He, Dandelion-like nickel/cobalt metal-organic framework based electrode materials for high performance supercapacitors, Journal of colloid and interface science, 531 (2018) 83-90.

[30] M.A. Ahsan, V. Jabbari, M.T. Islam, R.S. Turley, N. Dominguez, H. Kim, E. Castro, J.A. Hernandez-Viezcas, M.L. Curry, J. Lopez, J.L. Gardea-Torresdey, J.C. Noveron, Sustainable synthesis and remarkable adsorption capacity of MOF/graphene oxide and MOF/CNT based hybrid nanocomposites for the removal of Bisphenol A from water, The Science of the total environment, 673 (2019) 306-317.

[31] S. Rezaee, S. Shahrokhian, Facile synthesis of petal-like

NiCo/NiO-CoO/nanoporous carbon composite based on mixed-metallic MOFs and their application for electrocatalytic oxidation of methanol, Applied Catalysis B: Environmental, 244 (2019) 802-813.

[32] P. Horcajada, T. Chalati, C. Serre, B. Gillet, C. Sebrie, T. Baati, J.F. Eubank, D. Heurtaux, P. Clayette, C. Kreuz, J.S. Chang, Y.K. Hwang, V. Marsaud, P.N. Bories, L. Cynober, S. Gil, G. Ferey, P. Couvreur, R. Gref, Porous metal-organic-framework nanoscale carriers as a potential platform for drug delivery and imaging, Nature materials, 9 (2010) 172-178.

[33] R. Zhang, T. Zhou, L. Wang, T. Zhang, Metal-organic frameworks-derived hierarchical Co_3O_4 Structures as efficient sensing materials for acetone detection, ACS applied materials & interfaces, 10 (2018) 9765-9773.

[34] Y. Xiong, W. Xu, Z. Zhu, Q. Xue, W. Lu, D. Ding, L. Zhu, ZIF-derived porous ZnO-Co_3O_4 hollow polyhedrons heterostructure with highly enhanced ethanol detection performance, Sensors and Actuators B: Chemical, 253 (2017) 523-532.

[35] Y. Wang, M. Kong, Z. Liu, C. Lin, Y. Zeng, Morella-rubra-like metal–organic-framework-derived multilayered Co_3O_4/NiO/C hybrids as high-performance anodes for lithium storage, Journal of Materials Chemistry A, 5 (2017) 24269-24274.

[36] J. Deng, R. Zhang, L. Wang, Z. Lou, T. Zhang, Enhanced sensing performance of the Co_3O_4 hierarchical nanorods to NH_3 gas, Sensors and Actuators B: Chemical, 209 (2015) 449-455.

[37] I. Lee, S. Choi, H.J. Lee, M. Oh, Hollow Metal–organic framework microparticles assembled via a self-templated formation mechanism, Crystal Growth & Design, 15 (2015) 5169-5173.

[38] X. Liu, F. Zou, K. Liu, Z. Qiang, C.J. Taubert, P. Ustriyana, B.D. Vogt, Y. Zhu, A binary metal organic framework derived hierarchical hollow Ni_3S_2/Co_9S_8/N-doped carbon composite with superior sodium storage performance, Journal of Materials Chemistry A, 5 (2017) 11781-11787.

[39] H.-S. Lu, H. Zhang, X. Zhang, N. Sun, X. Zhu, H. Zhao, G. Wang, Transformation of carbon-encapsulated metallic Co into ultrafine Co/CoO nanoparticles exposed on N-doped graphitic carbon for high-performance rechargeable zinc-air battery, Applied Surface Science, 448 (2018) 369-379.

[40] T. Meng, Q.-Q. Xu, Z.-H. Wang, Y.-T. Li, Z.-M. Gao, X.-Y. Xing, T.-Z. Ren, Co_3O_4 nanorods with self-assembled nanoparticles in queue for supercapacitor, Electrochimica Acta, 180 (2015) 104-111.

[41] D. Ge, J. Peng, G. Qu, H. Geng, Y. Deng, J. Wu, X. Cao, J. Zheng, H. Gu, Nanostructured Co(ii)-based MOFs as promising anodes for advanced lithium storage, New Journal of Chemistry, 40 (2016) 9238-9244.

[42] J. Zhang, H. Lu, L. Zhang, D. Leng, Y. Zhang, W. Wang, Y. Gao, H. Lu, J. Gao, G. Zhu, Z. Yang, C. Wang, Metal–organic framework-derived ZnO hollow nanocages functionalized with nanoscale Ag catalysts for enhanced ethanol sensing properties, Sensors and Actuators B: Chemical, 291 (2019) 458-469.

[43] J. Hu, C. Zou, Y. Su, M. Li, Z. Yang, M. Ge, Y. Zhang, One-step synthesis of 2D C_3N_4-tin oxide gas sensors for enhanced acetone vapor detection, Sensors and Actuators B: Chemical, 253 (2017) 641-651.

[44] J. Cao, S. Wang, H. Zhang, T. Zhang, Constructing one dimensional Co_3O_4 hierarchical nanofibers as efficient sensing materials for rapid acetone gas detection, Journal of Alloys and Compounds, 799 (2019) 513-520.

[45] C. Su, L. Zhang, Y. Han, X. Chen, S. Wang, M. Zeng, N. Hu, Y. Su, Z. Zhou, H. Wei, Z. Yang, Glucose-assisted synthesis of hierarchical flower-like Co_3O_4 nanostructures assembled by porous nanosheets for enhanced acetone sensing, Sensors and Actuators B: Chemical, 288 (2019) 699-706.

[46] Y. Lin, H. Ji, Z. Shen, Q. Jia, D. Wang, Enhanced acetone sensing properties of Co3O4 nanosheets with highly exposed (111) planes, Journal of Materials Science: Materials in Electronics, 27 (2015) 2086-2095.

[47] W. Zhou, Y.P. Wu, J. Zhao, W.W. Dong, X.Q. Qiao, D.F. Hou, X. Bu, D.S. Li, Efficient gas-sensing for formaldehyde with 3D hierarchical Co_3O_4 derived from Co_5-based MOF microcrystals, Inorganic chemistry, 56 (2017) 14111-14117.

[48] Z. Jin, L.-P. Wang, Y. Zhang, J. Fan, M.-H. Liao, X.-F. Wang, Y. Ding, Highly sensitive and selective ethanol sensors based on porous Co_3O_4 nanobelts synthesized through a facile wet-chemistry method, Journal of Nanoparticle Research, 21 (2019).

[49] L.L. Wang, J.A. Deng, Z. Lou, T. Zhang, Nanoparticles-assembled Co_3O_4 nanorods p-type nanomaterials: One-pot synthesis and toluene-sensing properties,

Sens. Actuator B-Chem., 201 (2014) 1-6.

[50] T. Li, Z. Shen, Y. Shu, X. Li, C. Jiang, W. Chen, Facet-dependent evolution of surface defects in anatase TiO_2 by thermal treatment: implications for environmental applications of photocatalysis, Environmental Science: Nano, 6 (2019) 1740-1753.

[51] J.M. Xu, J.P. Cheng, The advances of Co_3O_4 as gas sensing materials: A review, Journal of Alloys and Compounds, 686 (2016) 753-768.

[52] N. Barsan, U. Weimar, Conduction model of metal oxide gas sensors, Journal of Electroceramics, 7 (2001) 143-167.

[53] Z. Zhang, L. Zhu, Z. Wen, Z. Ye, Controllable synthesis of Co_3O_4 crossed nanosheet arrays toward an acetone gas sensor, Sensors and Actuators B: Chemical, 238 (2017) 1052-1059.

Figure captions

Scheme. 1. Schematic illustration for the preparation process of Co_3O_4 nanospheres with different structures.

Fig. 1. (a) Digital photograph of the complete sensor; (b) schematic diagram for the structure of gas sensor device.

Fig. 2. XRD patterns of Co_3O_4 nanospheres at different calcination temperatures.

Fig. 3. FESEM images of (a, b) Co-MOF nanospheres; and Co_3O_4 products of (c, d) Co_3O_4-300; (e, f) Co_3O_4-400; (g, h) Co_3O_4-500.

Fig. 4. TEM images of (a) Co_3O_4-300; (b) Co_3O_4-400; (c) Co_3O_4-500; (d) HRTEM images of Co_3O_4-400, inset is the SAED image of Co_3O_4-400.

Fig. 5. Response of Co_3O_4 sensors to 100 ppm n-butanol at different temperatures.

Fig. 6. (a)Transient response curve of Co_3O_4 sensors; Response and recovery curves of (b) Co_3O_4-300, (c) Co_3O_4-400, (d) Co_3O_4-500 sensors to 100 ppm n-butanol at the optimal operating temperature.

Fig. 7. (a) sensing transient curves to different concentration of n-butanol at 140℃,the inset shows the enlarged dynamic sensing curves at n-butanol concentrations of 3 and 5ppm；(b)Response of Co_3O_4 samples to different ethanol concentrations;(c) The corresponding relationship between response and concentration;(d) Six periods of response–recovery curves to 100 ppm n-butanol at 140℃;(e) Responses of Co_3O_4 samples to different gases at at 140℃;(f) Long-term stability of the Co_3O_4-400 based

gas sensor.

Fig. 8. (a) XPS spectra of Co 2p for porous Co_3O_4 samples; XPS spectra of O 1s and curve-fitting for (b) Co_3O_4-300, (c) Co_3O_4-400, (d) Co_3O_4-500.

Fig. 9. The schematic diagram for gas sensing mechanism of the Co_3O_4 nanospheres based sensor.

Table1. Comparison of varied nanostructured Co_3O_4 in VOCs sensing performances.

Scheme 1.

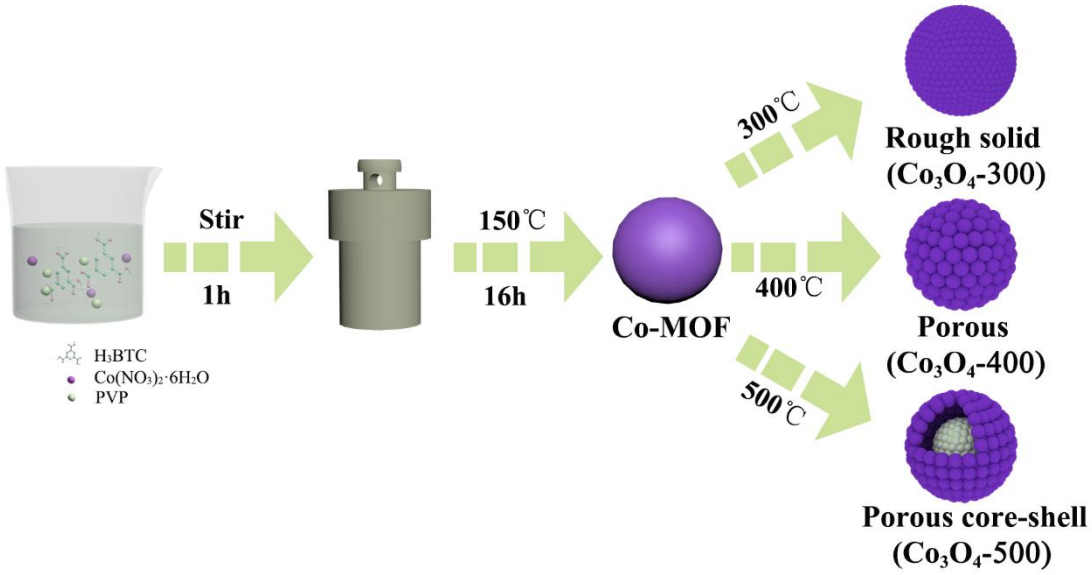
Stir
1h
150℃
16h
Co-MOF
300℃
Rough solid
(Co3O4-300)
400℃
Porous
(Co3O4-400)
500℃
Porous core-shell
(Co3O4-500)
H3BTC
Co(NO3)2·6H2O
PVP

Fig. 1.

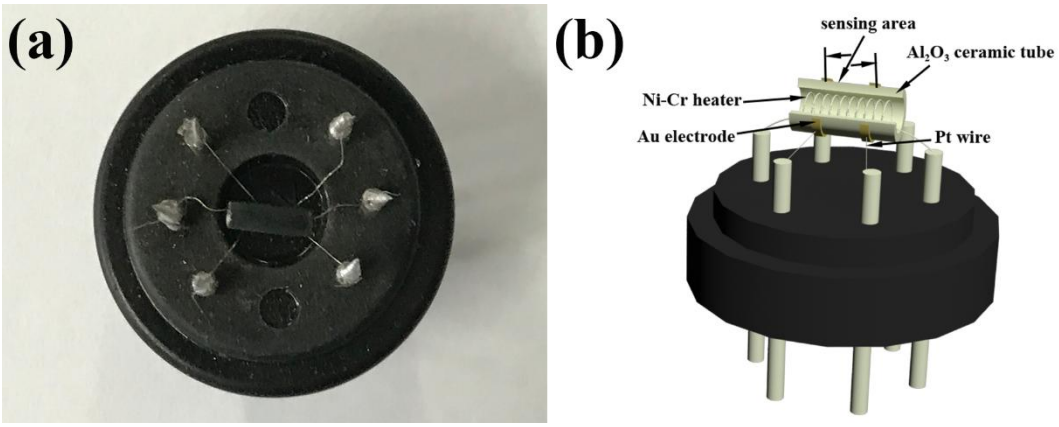
(a)
(b)
sensing area
Al_2O_3 ceramic tube
Ni-Cr heater
Au electrode
Pt wire

Fig. 2.

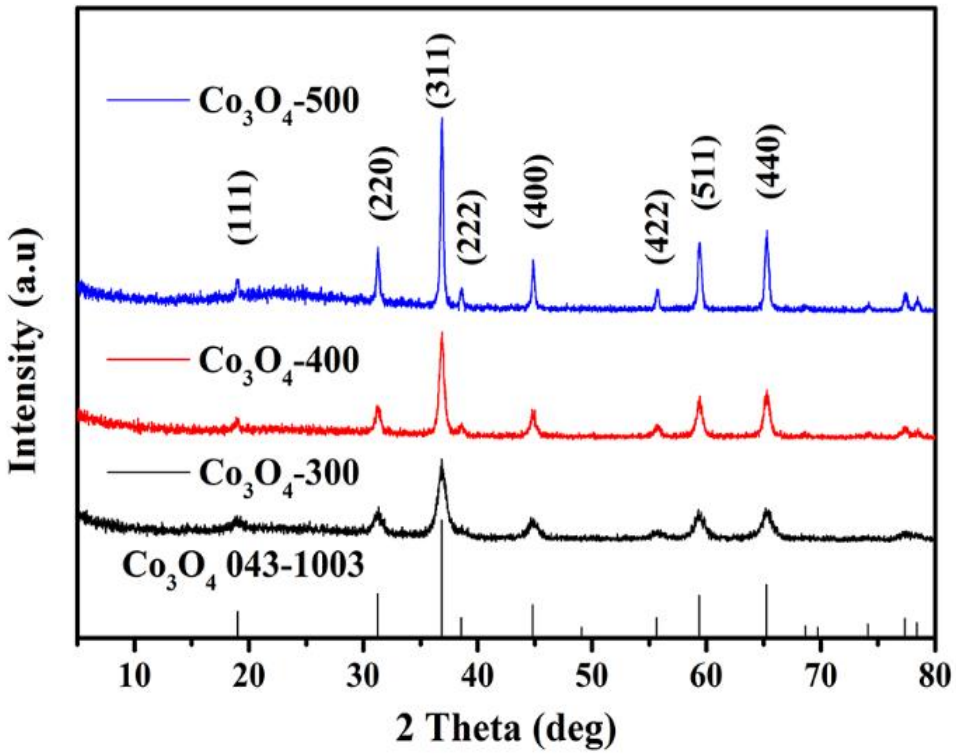
Co3O4-500
Co3O4-400
Co3O4-300
Co3O4 043-1003
(111)
(220)
(311)
(222)
(400)
(422)
(511)
(440)
Intensity (a.u)
2 Theta (deg)
10
20
30
40
50
60
70
80

Fig. 3.

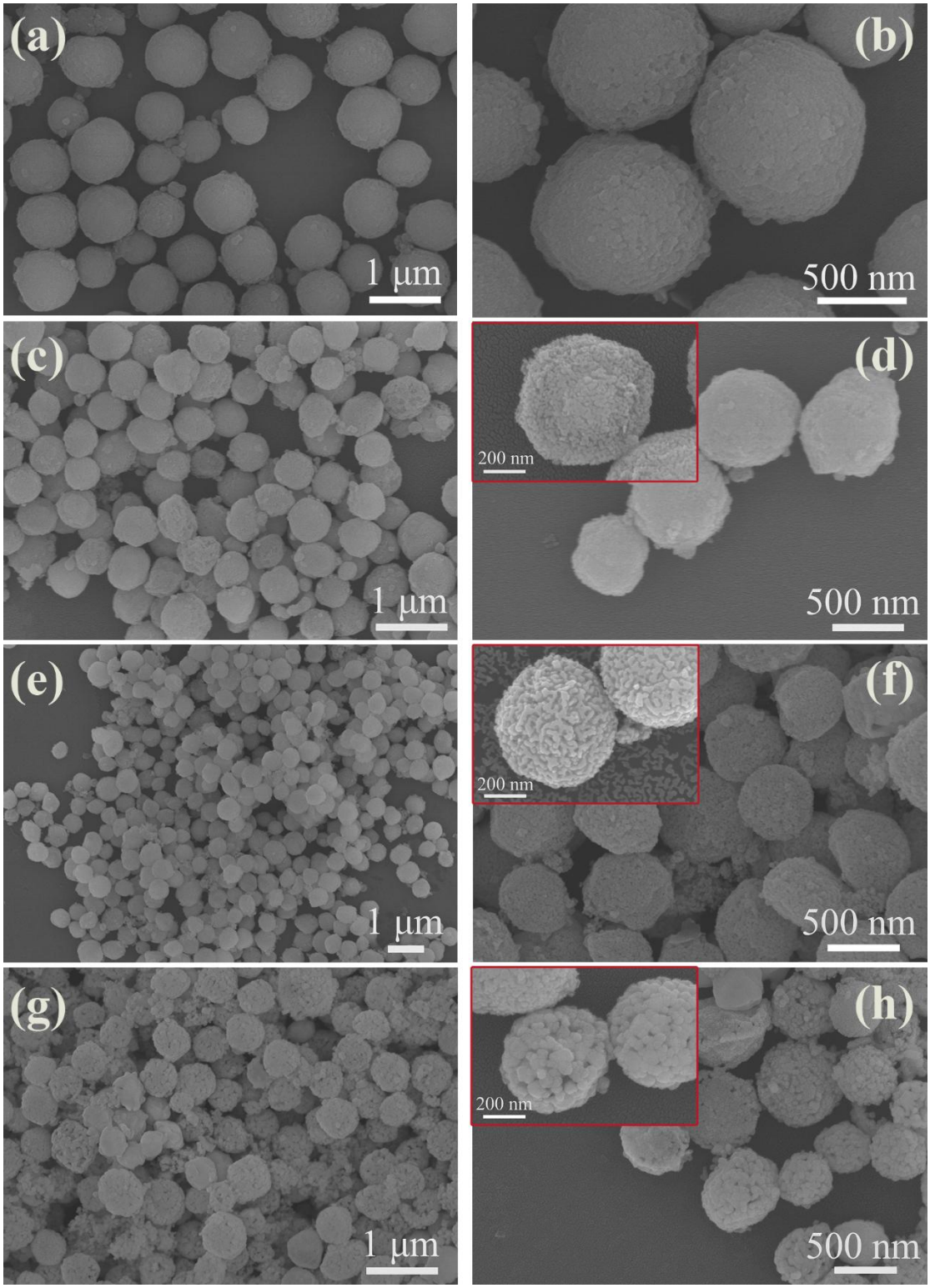
(a)
1 μm
(b)
500 nm
(c)
1 μm
(d)
200 nm
500 nm
(e)
1 μm
(f)
200 nm
500 nm
(g)
1 μm
(h)
200 nm
500 nm

Fig. 4.

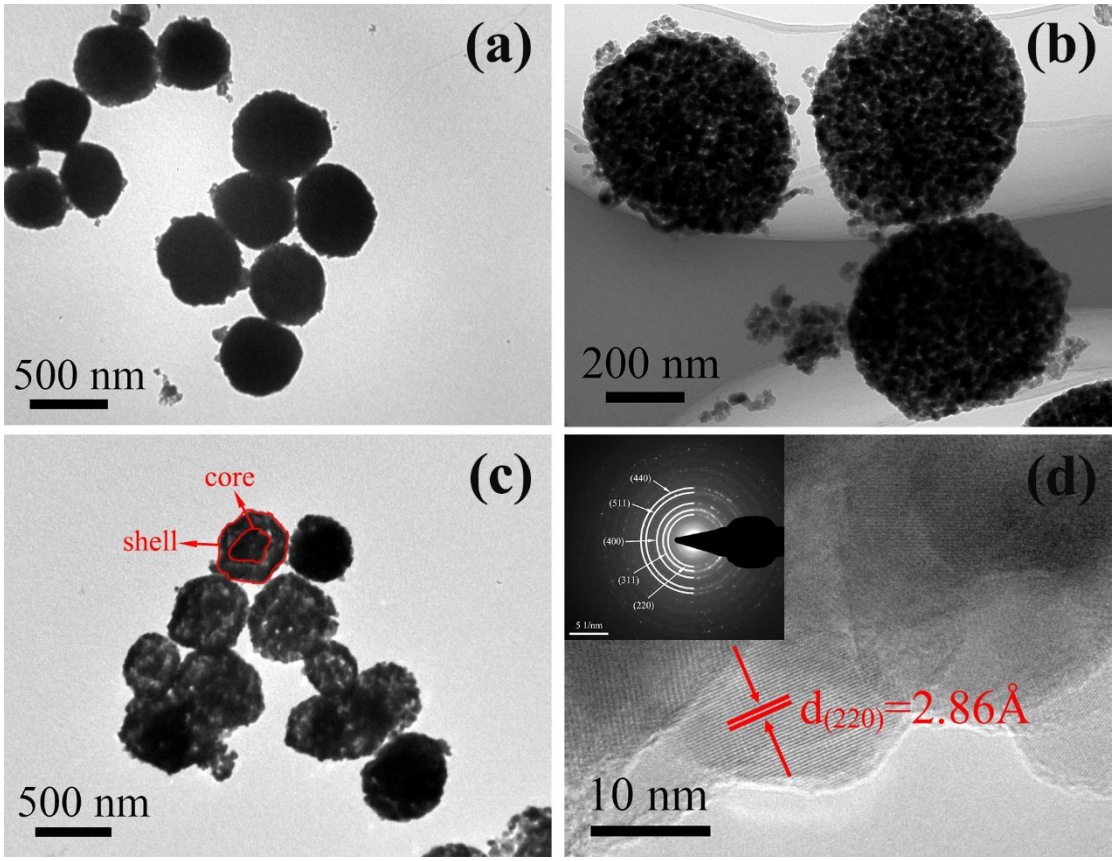
(a)
500 nm
(b)
200 nm
(c)
core
shell
500 nm
(d)
(440)
(511)
(400)
(311)
(220)
5 1/nm
d(220)=2.86Å
10 nm

Fig. 5.

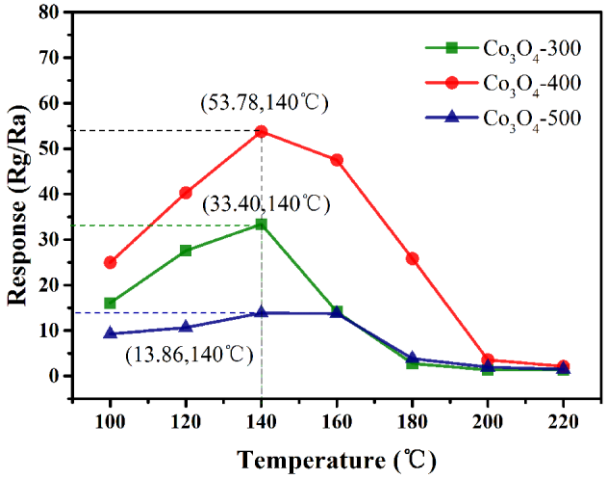
Response (Rg/Ra)
Temperature (℃)
Co3O4-300
Co3O4-400
Co3O4-500
(53.78,140℃)
(33.40,140℃)
(13.86,140℃)
80
70
60
50
40
30
20
10
0
100
120
140
160
180
200
220

Fig. 6.

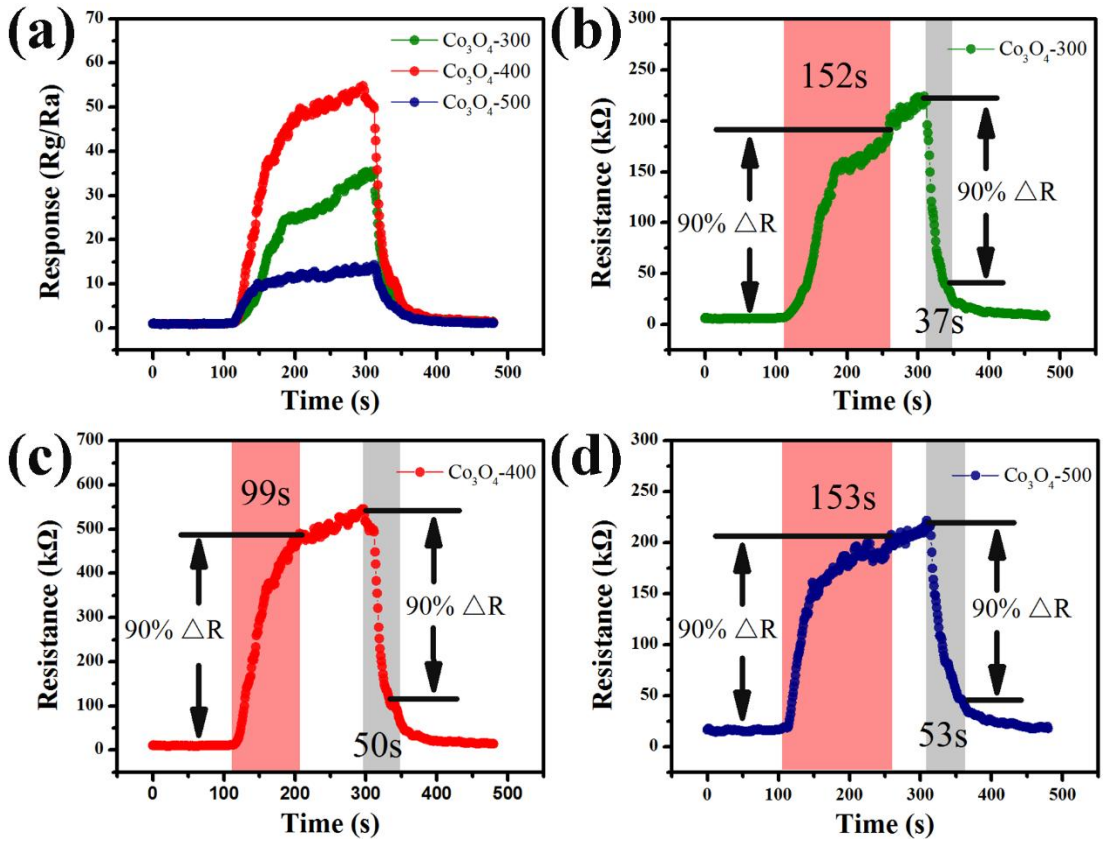
(a)
Response (Rg/Ra)
Time (s)
Co3O4-300
Co3O4-400
Co3O4-500
(b)
Resistance (kΩ)
Time (s)
Co3O4-300
152s
37s
90% △R
90% △R
(c)
Resistance (kΩ)
Time (s)
Co3O4-400
99s
50s
90% △R
90% △R
(d)
Resistance (kΩ)
Time (s)
Co3O4-500
153s
53s
90% △R
90% △R

Fig. 7.

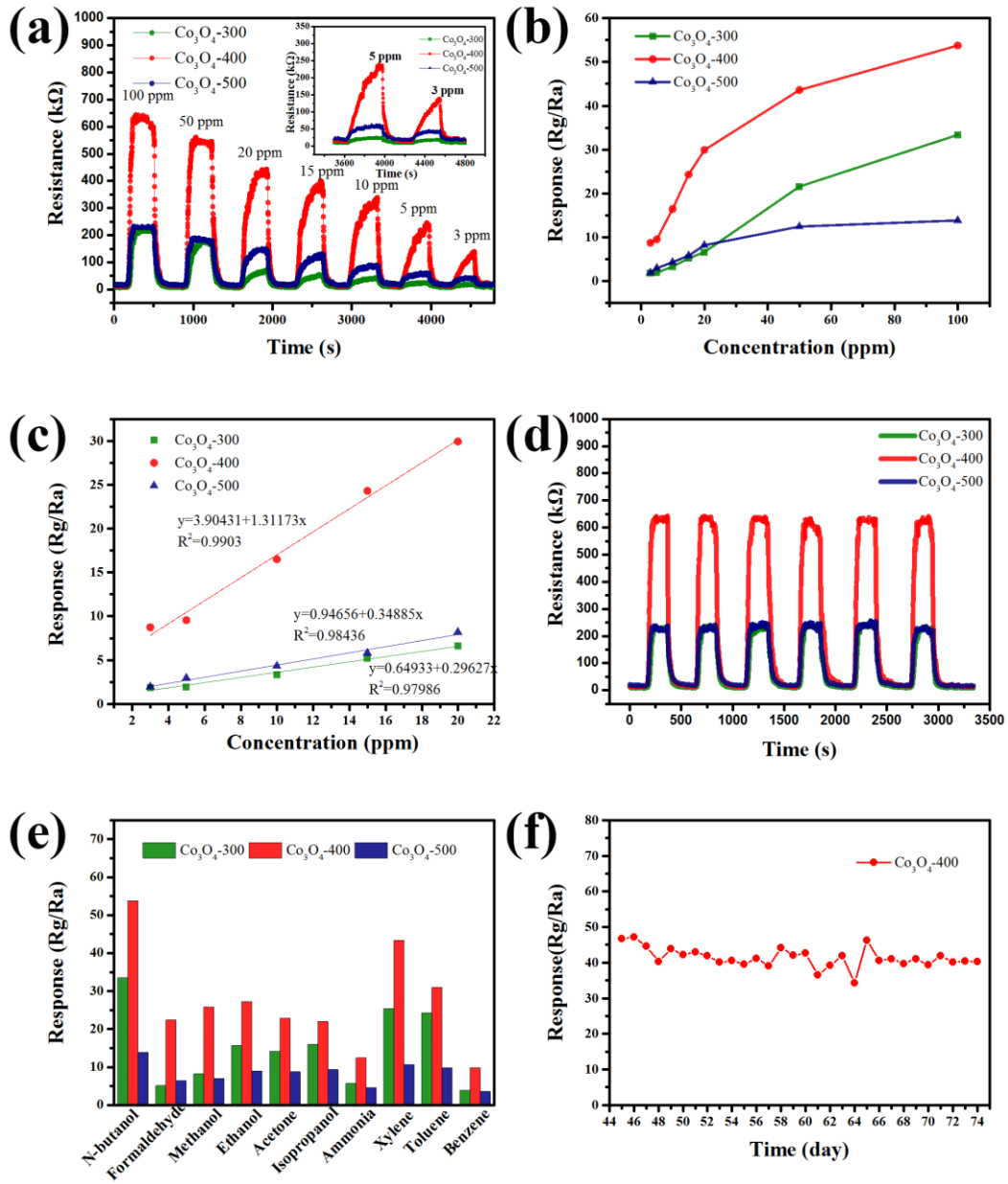
(a)
Co3O4-300
Co3O4-400
Co3O4-500
100 ppm
50 ppm
20 ppm
15 ppm
10 ppm
5 ppm
3 ppm
Resistance (kΩ)
Time (s)
(b)
Response (Rg/Ra)
Concentration (ppm)
(c)
y=3.90431+1.31173x
R2=0.9903
y=0.94656+0.34885x
R2=0.98436
y=0.64933+0.29627x
R2=0.97986
(d)
(e)
N-butanol
Formaldehyde
Methanol
Ethanol
Acetone
Isopropanol
Ammonia
Xylene
Toluene
Benzene
(f)
Response(Rg/Ra)
Time (day)

Fig. 8.

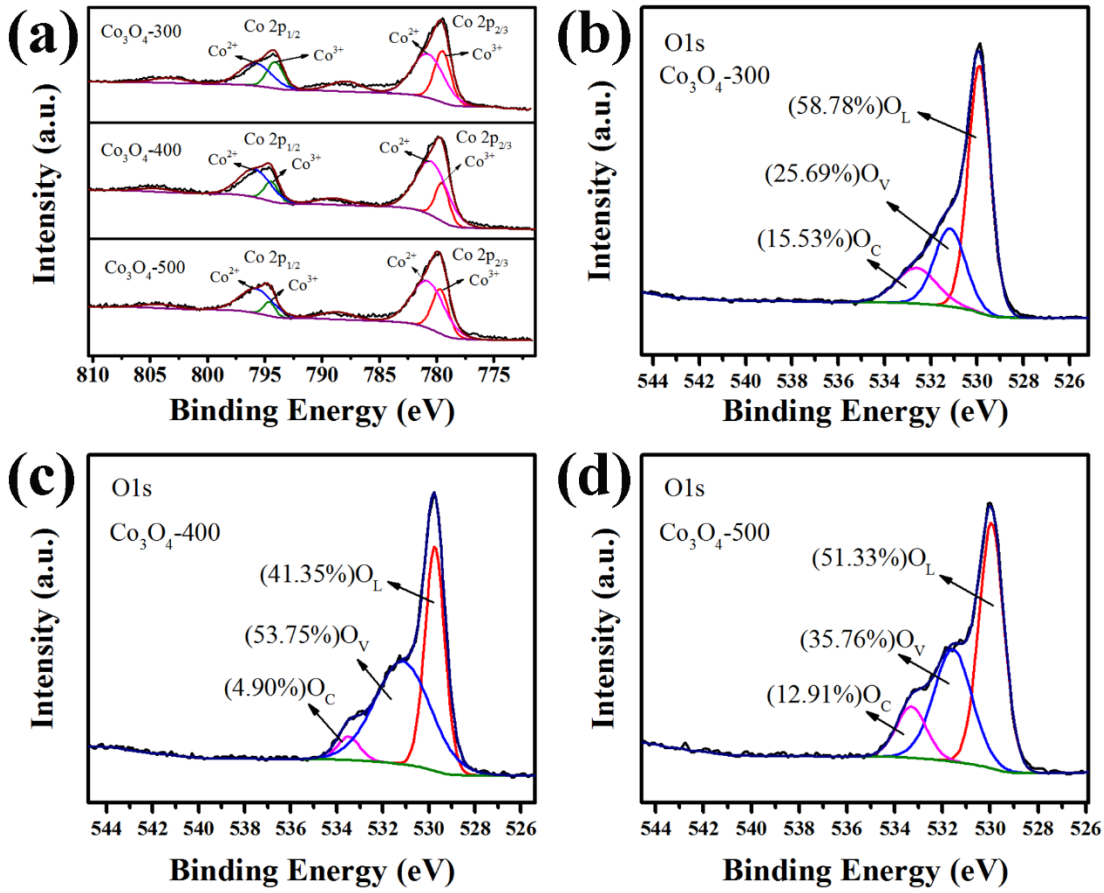
(a)
Co3O4-300
Co3O4-400
Co3O4-500
Co 2p1/2
Co 2p2/3
Co2+
Co3+
Intensity (a.u.)
Binding Energy (eV)
(b)
O1s
Co3O4-300
(58.78%)OL
(25.69%)OV
(15.53%)OC
(c)
O1s
Co3O4-400
(41.35%)OL
(53.75%)OV
(4.90%)OC
(d)
O1s
Co3O4-500
(51.33%)OL
(35.76%)OV
(12.91%)OC

Fig. 9.

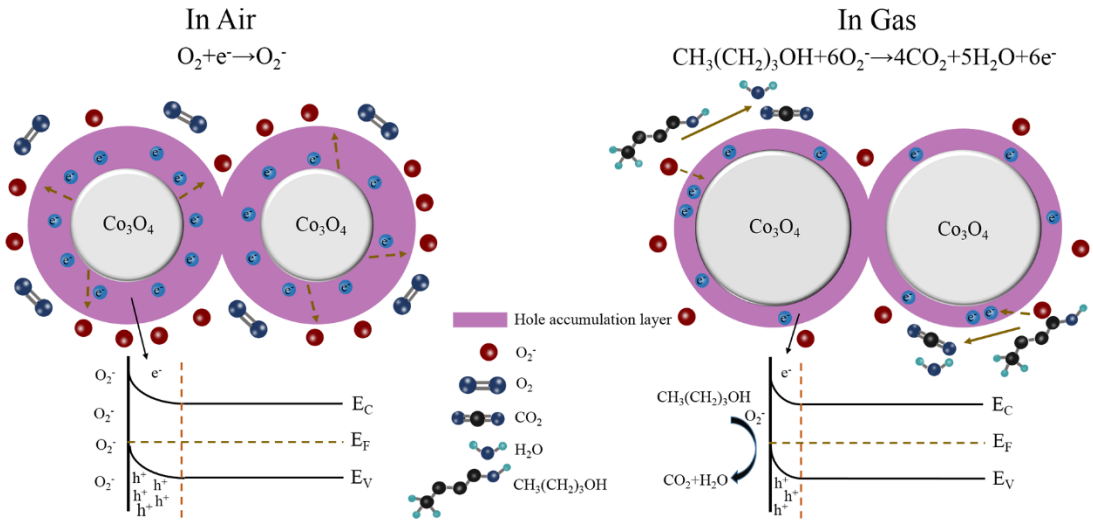
In Air
$O_2+e^-\rightarrow O_2^-$
In Gas
$CH_3(CH_2)_3OH+6O_2^-\rightarrow 4CO_2+5H_2O+6e^-$
Co_3O_4
Co_3O_4
Co_3O_4
Co_3O_4
Hole accumulation layer
O_2^-
O_2
CO_2
H_2O
$CH_3(CH_2)_3OH$
E_C
E_F
E_V
$CH_3(CH_2)_3OH$
CO_2+H_2O

Table1.

Materials	gas	Concentration (ppm)	Response (Rg/Ra)	Working temperature (℃)	Response/ Recovery time (s)	Ref.
Co_3O_4 hierarchical nanofibers	acetone	100	9.3	190	7/1	[44]
hierarchical flower-like Co_3O_4 nanostructures	acetone	100	48.1	130	18/13	[45]
Co_3O_4 nanosheets	acetone	100	6.1	160	98/7	[46]
3D Hierarchical Co_3O_4 spheres	formaldehyde	100	12	170	46/98	[47]
porous Co_3O_4 nanobelts	ethanol	100	20.3	300	15/20	[48]
Co_3O_4 nanorods	toluene	200	35	200	90/55	[49]
porous Co_3O_4 octadecahedron	n-butanol	100	21	100	146/90	[1]
porous Co_3O_4 nanospheres	**n-butanol**	**100**	**53.78**	**140**	**99/50**	**This work**

Graphic Abstract:

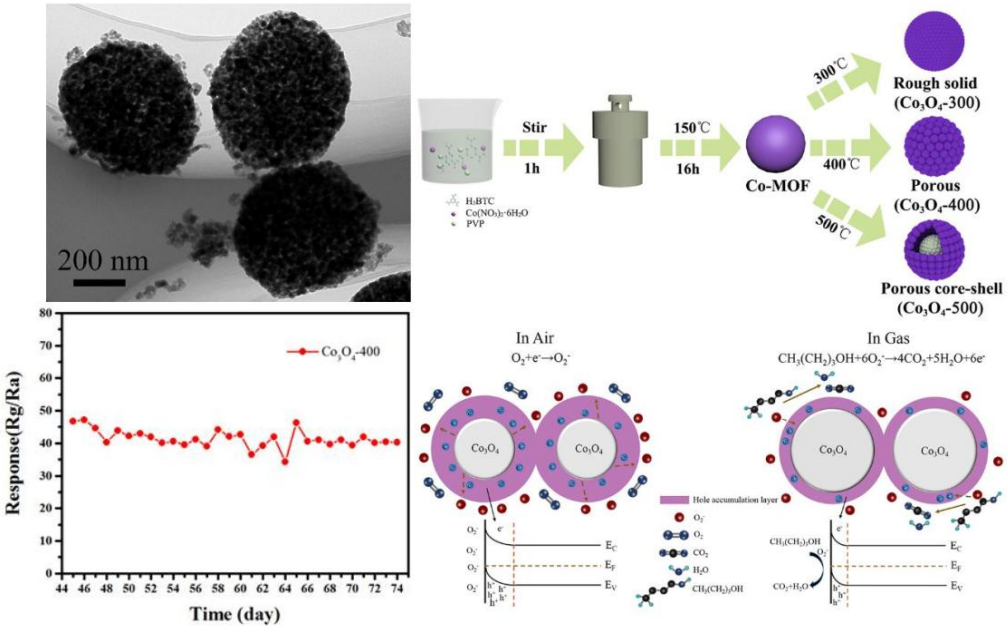

Highlights

- MOF-derived porous Co_3O_4 nanospheres with different microstructures were fabricated.
- The Co_3O_4-400 exhibits long-term stable and highly selective sensing performance for n-butanol.
- The excellent sensing performance of Co_3O_4-400 was attributed to its porous and rich oxygen vacancy microstructure.

Credit Author Statement

Lingli Cheng: Conceptualization, Methodology, Writing, Reviewing and Editing.

Yongchao He: Writing- Original draft preparation.

Maozhi Gong: Gas sensing performance test, Experimental supplement for Revised paper.

Xinhua He: Investigation.

Zhukai Ning: Software.

Hongchuan Yu: Language editing.

Zheng Jiao: Supervision

MOF-derived synthesis of Co_3O_4 nanospheres with rich oxygen vacancies for long-term stable and highly selective n-butanol sensing performance

Lingli Cheng[1*], Yongchao He[1], Maozhi Gong[1], Xinhua He[1], Zhukai Ning[1], Hongchuan Yu[3], Zheng Jiao[2]

1. *School of Environmental and Chemical Engineering, Shanghai University, Shanghai, 200444, P.R. China*
2. *Shanghai Applied Radiation Institute, Shanghai University, Shanghai 201800, PR China*
3. *National Centre for Computer Animation (NCCA), Bournemouth University, BH125BB, UK*

* Corresponding author:

[1]Lingli Cheng, *Email:* chenglingli@t.shu.edu.cn, Tel./fax: +86 21 66136229.

Abstract

Long-term stability and selectivity are crucial for the practical application of gas sensors, which are closely related to the microstructure and composition of sensor materials. In this work, Co-based metal organic framework (MOF) is used as a precursor and prepared by a simple hydrothermal method. After calcination, a series of Co_3O_4 nanospheres with various microstructures are derived. When the calcination temperature increases from 300℃ to 500℃, the microstructure of Co_3O_4 nanospheres changed from rough solid to porous, and then transformed into porous core-shell. When assembled into the gas sensors, the Co_3O_4 nanospheres with porous structure calcined at 400℃(Co_3O_4-400) show the highly selective response of 53.78 for 100 ppm n-butanol at the operating temperature of 140℃. Moreover, the theoretical limit of detection was calculated to be 150 ppb. The reproducibility, selectivity and stability of the gas sensor were further verified to be excellent. After 45 days, the response value of Co_3O_4-400 is at 86.74%, even after 75 days, the response value remains at 74.93%. The main reason can be attributed to the large specific surface area, abundant pore structure and a large number of oxygen vacancies on its surface. These findings provide reference for the development of p-type metal oxide semiconductor (MOS) sensors with long-term stability and high performance.

Keywords: Co_3O_4 porous structure; metal–organic frameworks; oxygen vacancies; long-term stability; Gas sensing; n-butanol

1. Introduction

In recent years, with the strengthening of environmental remediation, volatile organic compounds (VOCs) has received more and more attention. VOCs, which widely exist in the modern society, refer to the organic compounds that exist at room temperature in the form of gas, including ethanol, acetone, n-butanol, et al [1]. Due to their volatile nature at room temperature, VOCs are potentially harmful to human health. Such as n-butanol, an important chemical raw material, is mainly used for the preparation of plasticizers, surfactants, butyl acrylate, butyl acetate and ethylene glycol butyl ether. It is also used as a solvent for coatings and as an extractant for biochemicals. N-butanol is an irritant and can cause damage to the respiratory system and the skin. When people are exposed in the n-butanol environment, they may feel drowsy and dizzy [2, 3]. Therefore, it is necessary to develop high performance n-butanol gas sensor for human health and industrial environment monitoring.

Metal oxide semiconductors (MOS) are the most promising gas sensing materials for detecting VOCs, due to their low cost, excellent reliability, high sensitivity and environmental friendliness [4-6]. Metal oxide semiconductors are classified into n-type and p-type, and most of the researchers are focused on the n-type MOS, such as ZnO [7], SnO_2 [8, 9], In_2O_3 [10], WO_3 [11]. Recently, p-type MOS with unique surface redox properties and good catalytic properties are being extensively studied. Co_3O_4 is a typical p-type metal oxide semiconductor with a unique AB_2O_4 spinel structure. The transformation between different valence states of Co^{2+}/Co^{3+} endows

with the excellent gas sensitive reactivity of Co_3O_4 materials [12-15]. However, p-type metal oxide semiconductors generally have some drawbacks, such as low sensitivity and long response/recovery time [16-18]. Researchers have used substantial methods to solve the problems, such as changing the morphology and structure of the materials [1, 19, 20, 21], increasing their specific surface area and porosity [22, 23, 24], doping [25, 26], loading [27, 28], forming composite materials [6, 29, 30], and so on.

Metal–organic frameworks (MOFs) are a new class of porous materials composed by metal ions and organic ligands [31]. Due to its various topologies, tunable structure and pore size, ultra-high specific surface area, unique morphology and other excellent properties, MOFs have received extensive attention from researchers. In terms of energy storage [32], adsorption [33], catalysis [34], gas sensing [6], drug delivery [35], etc., MOFs have great application prospects. In the field of gas sensing, MOFs can be used as self-sacrificing templates to prepare hollow, core-shell or porous nanostructures by controlling thermolysis conditions to improve the performance of gas sensors [17, 20]. Morphology of materials is the main factor on determining their performance. For instance, Zhang et al. [36] reported that ZIF-67 was used as a precursor template to synthesize the core shell, porous core shell and porous popcorn structure of Co_3O_4 by controlling the calcination environment, which significantly improved its response to acetone. The porous ZnO-Co_3O_4 hollow polyhedral structure synthesized by Xiong et al. [37] has a response value of 106 to 1000 ppm ethanol at 200℃.Shi et al. [30] synthesized hollow Co_3O_4/In_2O_3 microtubules derived from MOFs to significantly improve the sensing performance of triethylamine, and the

response to 50 ppm TEA was 786.8. The above reports have demonstrated that metal oxides derived from MOFs generally have good morphology, large specific surface area, high porosity and more exposed active sites, which is benefit to improve the gas sensitivity of materials.

In this work, the nano-spherical Co-MOF was chosen as a self-sacrificial template, which was synthesized by a simple solvothermal method. Then, by controlling the calcination temperature, a series of Co_3O_4 samples with different microstructure and composition have been prepared. Through the performance tests, the relationship between microstructure and performance has been verified. The Co_3O_4 nanospheres calcinated at 400℃ (Co_3O_4-400) possess the best response sensitivity for n-butanol and long-term stability, which can be attributed to the porous and rich oxygen vacancies microstructure of it. Under the test temperature at 140℃, the response value of Co_3O_4-400 to 100 ppm n-butanol achieves 53.78, and the response value remains at 74.93% even after 75 days. Therefore, our work provides a facile MOF pyrolysis method for preparing long-term stable and high-performance gas sensitive MOS materials.

2. Experimental section

2.1 Materials

Cobalt nitrate hexahydrate ($Co(NO_3)_2 \cdot 6H_2O$,≥99%), polyvinyl pyrrolidone (PVP, M.W.30,000) and N,N-dimethylformamide (DMF) were purchased from Sinopharm Chemical Reagent.1,3,5-benzenetricarboxylic acid (H_3BTC) was obtained from Tokyo Chemical Industry. All chemicals used in this study were of analytical grade and

without any further purification.

2.2 Synthesis of Co_3O_4 nanospheres

Typically, 3.000g PVP was dissolved into the 60 mL DMF to form a clear solution. In the synthesis process, PVP acts as a stabilizer, which is beneficial to the formation of the spherical structure Co-MOF [38]. Then, 0.300g H_3BTC, 1.048g $Co(NO_3)_2 \cdot 6H_2O$ were added to the above solution under magnetic stirring vigorously for 1 hour. After that, the mixed solution was transferred into a 100 ml Teflon-lined stainless steel autoclave, and placed into an oven with a constant temperature of 150℃ for 16 h. The obtained purple product was collected and purified by centrifugation, washed several times with DMF and ethanol, and then dried at 60℃ overnight. Finally, the as-prepared Co-MOF was annealed in a Tube furnace at 400℃ for 2 h with a heating rate of 2℃/min in air. And then, the porous structure Co_3O_4 nanospheres were successfully prepared. The complete synthesis process was simulated in Scheme. 1. The black Co_3O_4 powder obtained by calcination at three different temperatures (300℃, 400℃, 500℃)in air was labeled as Co_3O_4-300, Co_3O_4-400 and Co_3O_4-500, respectively.

<**Scheme 1**>

2.3 Characterization

The crystallographic structure of the prepared Co_3O_4 samples were determined by X-ray diffraction (XRD, Rigaku D/max-2200, Japan). The morphologies and microstructure were investigated by field-emission scanning electron microscope (FESEM, Hitachi, S-4800, Japan) and transmission electron microscope (TEM, JEOL,

200CX, Japan). More detailed structural and crystal features were characterized by selected-area electron diffraction (SAED) and high-resolution TEM (HRTEM, JEOL, 2100F, Japan). The chemical components of the samples were investigated by X-ray photoelectron spectroscopy (XPS, Thermo, ESCALAB 250Xl, USA). The N_2 adsorption–desorption isotherms were measured on an automatic surface analyzer (Quantachrome, Quadrasord SI, USA). The surface area and the pore size distribution were evaluated using Brunauer–Emmett–Teller (BET) and Barrett–Joyner–Halenda (BJH) methods, respectively. The thermal decomposition behavior of the MOF precursor was studied by thermogravimetric analyzer (TGA, Mettler Toledo, TGA/DSC 3+, Switzerland).

2.4 Fabrication and measurements of gas sensors

The Co_3O_4 samples obtained by calcination at different temperatures were mixed with an appropriate amount of ethanol and ground to form a uniform paste. Then, the paste was applied to the surface of a hollow Al_2O_3 ceramic tube. The sample completely covered the area between the two gold electrodes on the surface of the ceramic tube. Subsequently, the ceramic tube coated with the sample was placed in an oven and dried at 60 ° C for 2 hours. Next, a Ni-Cr alloy heating wire was inserted into the ceramic tube, and the operating temperature was changed by adjusting the heating voltage. Finally, the heating wire and the two pairs of Pt wires on the ceramic tube gold electrode were welded to the sensor base to form a complete sensor device, as shown in Fig. S1. The sensing performance of the material was tested using the WS-30A gas sensor test system (Winsen Electronics Co., Ltd., Henan, China) as

shown in Fig.S2. Before the test, the sensor was aged at 300 ° C for 2 days on an aging device to improve the stability of its sensing performance. The gas response (sensitivity) is defined as $S=R_g/R_a$, where R_g is the resistance of the sensor in the target gas and R_a is the resistance in ambient air. The response of the sensor is the relative change in resistance of the material in the air and in the target gas [16]. The response and recovery times are defined as the time required for the sensor to reach 90% of the total resistance change during the process of adsorbing and desorbing the target gas, respectively [39].

3. Results and discussion

3.1. Structural and morphological characteristics

The Co-MOF was used as the precursor, and a series of Co_3O_4 nanospheres were synthesized by calcinating at different temperature. The XRD pattern of Co-MOF is shown in Fig. S3, revealing that the Co-MOF precursor is a crystalline material, which is consistent with the results reported by previous researchers [40, 41]. Subsequently, the morphological and structural changes of Co-MOF-derived metal oxide Co_3O_4 at different calcination temperatures were investigated.

< **Fig. 1**>

The corresponding powder X-ray diffraction (XRD) patterns of the calcined products can provide information on the crystallinity and phase composition, as shown in Fig. 1. The XRD patterns of the three samples all have identical diffraction peak positions and similar peak shapes, which are in good agreement with the cubic spinel structure of Co_3O_4 (JCPDS no. 043-1003), indicating that the Co-MOF had

been successfully converted into Co_3O_4. The diffraction lines are located at 2θ =19.0, 31.3, 36.8, 44.8, 59.4, 65.2° marked by their index's planes ((1 1 1), (2 2 0), (3 1 1), (4 0 0), (5 1 1), (4 4 0)), respectively. No other impurity peaks were detected, indicating that the Co_3O_4 samples are of high purity, and the strong peaks and spikes of the samples also confirm the high crystallinity. The change of the calcination temperature only changed the crystallinity of the products, but had no effect on the composition. Among the three kinds of Co_3O_4 samples, Co_3O_4-500 has the best crystallinity and the strongest diffraction peak intensity followed by Co_3O_4-400. And Co_3O_4-300 has the lowest crystallinity.

< **Fig. 2**>

The morphologies of the precursor and products were characterized by field emission scanning microscopy, as shown in Fig. 2. Fig. 2(a) shows that the synthesized Co-MOF is about 600 nm-900 nm in diameter, and the particles formed are relatively uniform. As observed in Fig. 2(b), the as-prepared Co-MOF precursor has a regular spherical structure and the surface is slightly rough. Fig. 3(c-h) exhibits the FESEM image of Co_3O_4 samples at different calcination temperatures. For the calcined sample at 300℃, Fig. 2 (c, d) show the spherical structure similar to that of the Co-MOF precursor, and the morphology remained intact. As observed from the inset in Fig. 2(d), the Co_3O_4-300 sample has a rougher surface than the precursor, which was mainly caused by thermal decomposition of the organic ligand. When the calcination temperature was raised to 400℃, Co_3O_4-400 still maintained a complete spherical shape, as shown in Fig.2 (e, f). It can be seen from Fig. 2(f) and its inset that

the surface roughness of the Co_3O_4 sample is further increased, and the particle size is gradually reduced to a diameter of about 500 nm. At the same time, the framework structure exhibits a complete sphere composed of ~25nm tiny nanoparticles, and the pore diameter is further increased. When the calcination temperature was 500℃, the Co_3O_4-500 sample produced ~50nm nanoparticles during the formation process, and significant large pores can be seen between the tiny nanoparticles, as shown in Fig. 2 (g, h). Compared to Co_3O_4-400, the nanoparticles constituting the Co_3O_4-500 sample are larger in size, resulting in an increase in pores between the particles. The calcination temperature was increased from 300℃ to 500℃, the Co_3O_4 products were able to maintain a complete spherical morphology, but the surface became rougher and the pores became larger.

< **Fig. 3**>

In order to further study the microstructure changes of Co_3O_4 products affected by calcination temperature, TEM and HRTEM were used to characterize the samples. In Fig. 3(a), the internal structure of the Co_3O_4-300 sample is in a solid state, and no obvious porous structure can be observed. Fig. 3(b) shows that a large number of pores can be identified on the surface of Co_3O_4-400, and the porous nanospheres were successfully prepared. When the calcination temperature was raised to 500℃, the porous structure gradually transformed into the core-shell structure and the internal pore size increased, as shown in Fig. 3(c). When the calcination temperature increased from 300℃ to 500℃, the structure of the products changed from the rough solid structure to the porous structure, and then further transformed into the porous

core-shell structure. The formation of a large number of pores in the products are due to the organic ligands being oxidized to CO_2 and H_2O and volatilized into the air. Moreover, it can be seen from the HRTEM in Fig. 3(d) that the lattice fringes of the Co_3O_4-400 sample is 2.86 Å, which corresponds to the (220) crystal planes of spinel Co_3O_4. The selected area electronic diffraction (SAED) pattern (inset image of Fig. 3(d)) exhibits several concentric rings, indicating that the Co_3O_4-400 spherical nanostructure is polycrystalline in nature and has good crystallinity.

In addition, the thermal decomposition behavior of the Co-MOF precursor was first studied by thermogravimetric analysis (TG) and differential thermal analysis (DTA), as shown in Fig. S4(a). Below 150℃, the mass loss is about 8.1%, mainly to remove adsorbed water molecules, gases and solvents. The tricarboxylate linkers gradually decomposed in the temperature range of 150℃ to 300℃. From 300℃ to 450℃, the apparent mass loss is 48.8%, indicating that the organic ligands decomposed and the metal-organic frameworks were completely converted into the metal oxides. Such a significant mass reduction means that a large amount of gas (CO_2, H_2O) was produced in the process of decomposing the organic matter [42-44]. According to the DTA analysis, the corresponding exothermic peak appeared at 389℃. When the pyrolysis temperature exceeded 450℃, the sample quality remained substantially stable. Fig. S4(b) shows the TG analysis curves of Co_3O_4-300, Co_3O_4-400 and Co_3O_4-500, respectively. The mass loss of the three samples is within 3.5%, indicating that the residual carbon content in all the samples is very low and the purity of samples is high.

Nitrogen adsorption-desorption isotherms were conducted in order to identify the specific surface areas and porosity structure of as-synthesized Co_3O_4 nanospheres, and the results are shown in Fig. S5. The N_2 adsorption-desorption curves of all products show typical IV isotherms with H3 hysteresis loop, indicating the presence of the mesoporous structure. With the increment of calcination temperature, the specific surface area of Co_3O_4 samples decreased. The Co_3O_4-300 sample has the largest specific surface area of 69.8 m^2/g, while Co_3O_4-400 and Co_3O_4-300 are 39.3 m^2/g and 17.8 m^2/g, respectively. The pore size distribution calculated by the BJH method is shown in the inset of Fig. S5. The average pore diameters of Co_3O_4-300 and Co_3O_4-400 are 10.5 nm and 23.6 nm, respectively. And the pore sizes of Co_3O_4-500 are mainly distributed around 3.1 nm and 41.8 nm. As the calcination temperature increases, the pore size of the Co_3O_4 product increases, which is consistent with the results observed in the SEM. The results of various characterizations show that the calcination temperature has a significant effect on the structure and morphology of Co_3O_4 nanospheres formed by self-assembly of nanoparticles, especially with MOF as a self-sacrificing template.

3.2. Gas sensing properties

< **Fig. 4**>

The gas sensing performance of as prepared Co_3O_4 samples were evaluated through testing the working temperature, response value, response/recovery time, stability and selectivity. The working temperature is an important indicator to measure the performance of gas sensors, which is of great significance for the practical application

of sensors. Fig. 4 depicts the response of three Co_3O_4 samples to 100 ppm n-butanol over a range of 100℃-220℃. From 100℃ to 140℃, the response of these three sensors increases with the increment of operating temperature until the maximum response at 140℃ is obtained. The Co_3O_4-400 sample exhibits the highest response of 53.78 for 100 ppm n-butanol at 140℃, comparing with 33.40 for Co_3O_4-300, and 13.86 for Co_3O_4-500. Subsequently, when the operating temperature increases, the response decreases gradually. This phenomenon can be attributed to the following reasons [12]. At first, when the operating temperature is relatively low, most target gas is inactive, as well as there is not enough activation energy to react with the surface-adsorbed oxygen species, which leads to a low response. As the temperature increases, the gas molecules obtain enough energy to overcome the activation energy barrier, so the response enhances. Then, when the temperature exceeds the optimum reaction temperature, the desorption rate of the gas molecules on the surface of sensing materials is greater than the corresponding adsorption rate, which causes the response value diminish greatly. Therefore, the sensor exhibits the response characteristics of "increase-maximum-decrease" [45]. The optimal operating temperature can be determined to be 140℃, which is critical for subsequent gas-sensitive performance tests.

< **Fig. 5**>

The transient sensing curves of the three sensors for 100ppm n-butanol at the optimum operating temperature are shown in Fig. 5(a). All the sensors show similar response and recovery processes. Fast response and recovery processes are very

important for the practical application of gas sensors. The response and recovery time are calculated and labeled in Fig. 5(b, c, d). The response times of Co_3O_4-300, Co_3O_4-400, and Co_3O_4-500 are 152s, 99s, and 153s, respectively, and the recovery times are 37s, 50s, and 53s, respectively. Comparing with Co_3O_4-300 and Co_3O_4-500, Co_3O_4-400 has a much shorter response time, but its recovery time is slightly longer than that of Co_3O_4-300.

< **Fig. 6**>

Fig. 6 (a) is the typical dynamic sensing transient curves of Co_3O_4 sensors at different n-butanol concentrations (3ppm-100ppm). All the sensors showed good response, and the response value enhanced with the increment of n-butanol concentration. The relationship of response values and n-butanol concentrations for three samples are displayed in Fig. 6(b). When the concentration of n-butanol is 3ppm, the response of Co_3O_4-300, Co_3O_4-400 and Co_3O_4-500 are 1.87, 8.74 and 1.94, respectively. It is obvious that Co_3O_4-400 has the lowest detection limit in the three sensors. Meanwhile, the Co_3O_4-400 exhibits the highest response value at each n-butanol concentration. It can also be observed in Fig. 6(b) that the response value of the Co_3O_4-400 sample increases significantly in the concentration range from 3 ppm to 20 ppm, and then it gets saturated. The linear relationship between n-butanol concentration and the response values in the range from 3 ppm to 20 ppm is shown in Fig. 6(c). The theoretical detection limits for n-butanol in Co_3O_4 samples can be evaluated through linear extrapolation, the calculating of the LOD is LOD = 3 × (Standard Deviation/Slope), which are calculated to be 215 ppb, 150 ppb, and 190

ppb, respectively [46]. The above results indicate that the Co_3O_4-400 sample owns excellent sensitivity for n-butanol, which means that it has great application potential in low concentration n-butanol sensing.

Stability (repeatability) is crucial for a sensor in the commercial application. To test the stability of Co_3O_4 sensors, they were measured over 6 periods (a period means a complete cycle of response and recovery procedures to 100 ppm n-butanol). The sensing transient curves are shown in Fig. 6(d). During 6 periods, the instantaneous response values of the sensors have no obvious change, which proves the good reversibility and repeatability of the Co_3O_4 sensors prepared in our work.

Selectivity is another important factor for the practical application of gas sensors. The response of all Co_3O_4 samples toward 100 ppm VOCs mixture (including n-butanol, formaldehyde, methanol, ethanol, acetone, isopropanol, ammonia, xylene, toluene, benzene, sulfur dioxide and nitrogen Dioxide) is shown in Fig. 6(e). The Co_3O_4-400 sample not only shows the highest response to all the VOCs, but also exhibits the best selectivity to n-butanol. The response value of Co_3O_4-400 to n-butanol is 1.3-5.5 times than other VOCs. Among them, only xylene could make interference with n-butanol, which may be due to similar optimal operating temperature and chemical reactivity energy. Moreover, in order to evaluate the selectivity of all Co_3O_4 sensors to oxidizing gases (such as SO_2 and NO_2), the responses of the Co_3O_4-300, Co_3O_4-400 and Co_3O_4-500 sensors to 100 ppm SO_2 and NO_2 were tested. As shown in Fig. 6(e), Co_3O_4-300, Co_3O_4-400 and Co_3O_4-500 sensors show extremely low response to SO_2 and NO_2 at the optimal operating

temperature as 140℃. It means all Co_3O_4 sensors exhibit the best selectivity to n-butanol among all examined gases at the operating temperature at 140℃.

The selectivity of Co_3O_4-400 to n-butanol has been analyzed in details. The reasons for the selectivity of Co_3O_4-400 to n-butanol include two points: (i) The polarity of hydroxyl group (-OH) is stronger than amino group (-NH2), aldehyde (-CHO), carbonyl group (-C=O) and phenyl group. For containing hydroxyl group, the polarity of n-butanol is stronger than ammonia, formaldehyde, acetone, xylene, toluene and benzene. That means n-butanol has a very strong ability to provide electrons. And the large intrinsic crystal defects and rich oxygen vacancies of Co_3O_4-400 make it prefer to bound extra electrons as free carries, so it shows good selectivity to n-butanol. Furthermore, the excellent electron donor characteristics of n-butanol causes it react with the adsorbed oxygen species at the relatively low concentration, exhibiting relatively high response. (ii) The diffusivity determines the residence time of the detected gas on the surface of gas sensor. And the longer residence time can improve the response of gas sensors to the detected gas. Comparing with ethanol and methanol, n-butanol has a lower diffusivity for its higher molecular weight. Hence, the residence time of n-butanol on Co_3O_4-400 is longer than other detected gases, which endows n-butanol higher response.

Long-term stability as a significant impact on the durability of sensors has been tested. In order to evaluate the influence of the external environment on the stability of the gas sensor, the Co_3O_4-400 sensor was placed in the air for 45 days. After 45 days, the response value of Co_3O_4-400 to n-butanol still can achieve 46.65, which was

86.74% of the initial value, and show good response-recovery performance, indicating that the stability of Co_3O_4-400 is splendid. Then, the response of the Co_3O_4-400 to 100 ppm n-butanol at 140℃ was continuously tested for 30 days , as shown in Fig.6(f). Within 30 days, the response of the Co_3O_4-400 sensor fluctuated slightly. After the 75 days' test, the response value of the Co_3O_4-400 is tested to be 40.30, retaining 74.93% without significant reduction, further indicating that it has good long-term stability and guarantees its service life. Furthermore, the Co_3O_4-400 sensor synthesized in this work is compared with the reported Co_3O_4 sensors. The results are listed in Table 1. It can be seen from this, the gas sensor prepared in this work can effectively enhance the response of n-butanol and reduce the operating temperature. Considering the response and the optimal operating temperature, the unique 3D porous structure Co_3O_4 nanospheres gas sensor shows superior gas sensing properties and has great practical application potential.

< **Table 1**>

3.3. Gas sensing mechanism

< **Fig. 7**>

The reaction process of the target gas on the surface of the material plays an important role in the sensing process. In order to further study the electronic states of the surface elements, the XPS analysis of Co_3O_4 samples was performed. Fig. 7(a) shows the high-resolution spectrum of Co 2p, in which there are two characteristic peaks and two satellite peaks. Both the positions and distributions of the Co 2p XPS peaks in all the Co_3O_4 samples are similar. Two characteristic peaks at 779.8 eV and

794.9 eV belong to the Co $2p_{3/2}$ and Co $2p_{1/2}$ spin-orbital peaks of Co_3O_4, respectively, and their corresponding satellite peaks are at 789.7 eV and 804.6 eV. The difference between Co^{2+} and Co^{3+} peaks can be observed after curve-fitting, as shown in Fig. 7(a). Fig. 7 (b-d) show the high resolution XPS spectra of O1s for Co_3O_4 samples. These spectra can be divided into three fitted peaks, corresponding to O_L, O_V and O_C, respectively. O_L refers to the lattice oxygen species, which contributes little to the gas response for its stability. O_V means that there are oxygen vacancies on the surface of samples, which can provide active sites for the gas adsorption and reaction on the surface of sensing materials. O_C represents the chemically adsorbed oxygen species, such as O_2^-, O^-, O^{2-}. When the calcination temperature is 300℃, 400℃, and 500℃, the corresponding O_V contents are 25.69%, 53.75%, and 35.76%, respectively. Obviously, Co_3O_4-400 has the highest oxygen vacancy content, which leads to its highest response to 100 ppm n-butanol at 140℃. Heat treatment is one of the common methods for the controllable defect generation of nanomaterials, and it can be adjusted by controlling the calcination temperature and the atmosphere. The defects due to heat treatment are mainly the result of the release and recovery of O atoms in the material lattice. Therefore, in the presence of oxygen, the oxygen vacancy concentration will have a high point [53]. The presence of surface oxygen vacancies plays a crucial role in chemical sensing. Positively charged oxygen vacancies tend to trap electrons, effectively separating electron-hole pairs and improving sensing performance. The oxygen vacancy content of Co_3O_4-300 is 25.69 %, which is lower than 35.76 % of Co_3O_4-500, but Co_3O_4-300 has higher response to 100ppm n-butanol. This may be

due to the fact that the specific surface area of Co_3O_4-300 is much larger than that of Co_3O_4-500.

The other major factor affecting gas sensing performance is specific surface area and pore size. In general, a large specific surface area enables the sensing material to adsorb more oxygen species. The Co_3O_4-400 sample has a specific surface area of 39.3 m^2/g. Meanwhile, the porous structure of Co_3O_4-400 provides a large amount of exposed area for gas sensing, which is conducive to improving its sensing performance of n-butanol. According to surveys, the average pore size of many metal oxide sensing materials is around 25 nm [8, 25, 48, 50]. The unique porous structure of the product and the appropriate pore size facilitate the penetration of gas molecules into the interior of the sensing material. This allows the hole accumulation layer to be formed on both the outer layer and the inner layer of the materials, resulting in a low initial resistance in the air.

Furthermore, the good catalytic activity of Co_3O_4 also plays a positive role in improving gas sensitivity, in which Co^{3+} is capable of oxidizing reductive gases [29]. During the catalytic process, the reductive gas reacts with oxygen ions adsorbed on the Co^{3+} active site, causing a change in resistance and generating Co^{2+}. Then Co^{2+} can be oxidized to active Co^{3+} by the gaseous oxygen molecule in the air. In the target gas, Co^{3+} in Co_3O_4 can promote the oxidation reaction of n-butanol, improving the sensing performance. In summary, the excellent gas sensing performance of the Co_3O_4-400 material for n-butanol can be attributed to the following three factors: (i) abundant oxygen vacancies; (ii) the unique porous structure with a large specific

surface area; (iii) Catalytic activity of Co_3O_4 for n-butanol.

< **Fig. 8**>

The sensing characteristics of MOS-based gas sensors are affected by the surface reaction of the sensor layer. The sensing mechanism of p-type semiconductor oxide Co_3O_4 is closely related to the change of resistance. However, the change in resistance is mainly due to the change in the concentration of holes in the surface region [54]. As shown in Fig. 8, when the Co_3O_4 sensor is exposed to the air, oxygen molecules are adsorbed on the surface of Co_3O_4, and electrons (e^-) are trapped from the conduction band to form different oxygen species (such as O_2^-, O^-, O^{2-}). O^- is formed between 100℃and 300℃ [55]. The optimum operating temperature of the Co_3O_4 sensor in this work is 140℃, so the main oxygen species is O^- (Eq. (1)). With the changing of adsorbed oxygen species, the electron depletion layer of Co_3O_4 is generated and the hole concentration is increased to form the hole accumulation layer [56]. Since the majority carrier of Co_3O_4 is hole, the resistance of Co_3O_4 in the air is low. When the n-butanol gas is injected, the adsorbed oxygen species (O^-) react with the reductive n-butanol (Eq. (2)). The electrons generated in this process return to the conduction band of Co_3O_4, causing the electron-hole pairs recombine, the hole accumulation layer shrink, and the resistance of materials increase. The recovery process is just the reversible process of the above reaction. When the n-butanol gas is removed, the oxygen molecules again capture electrons from the conduction band, reducing the resistance to its initial value.

$$O_2 + 2e^- \rightarrow 2O^- \qquad \text{Eq. (1)}$$

$$CH_3(CH_2)_3OH + 12O^- \rightarrow 4CO_2 + 5H_2O + 12e^-$$ Eq. (2)

4. Conclusion

The porous structure Co_3O_4 was successfully prepared by the precursor derivatization strategy of metal-organic framework and applied to gas sensing. Through performance test, the Co_3O_4-400 exhibits the best gas sensitivity. At the optimum testing temperature, the response to 100 ppm n-butanol is 53.78 and the theoretical limit of detection is 150 ppb. Co_3O_4-400 also owns good stability and reproducibility. After six consecutive cycles of testing, there was no significant change in the response curve to n-butanol. After left in the air for 45 days, the response value of Co_3O_4-400 to n-butanol was tested to be 46.65, which was 86.74% of the initial value. Even in the following 30-day long-term test, the response value was still stable, retaining 74.93% of the initial value. The unique spherical porous microstructure make Co_3O_4-400 have a large specific surface area and a suitable pore size. The larger specific surface area can adsorb a large amount of gas, and the proper pore size is conducive to the diffusion of gas molecules into the sensing material, thereby helping to improve the gas sensing performance. Additionally, the abundant oxygen vacancies generated by the heat treatment provide a large number of active sites and also help to improve the sensing performance. Our work provides a strategy for developing p-type semiconductor metal oxide sensors with high response, low detection limit and low temperature.

Acknowledgements

L.L. Cheng, Y.C. He and G.M. Zhi contributed equally to the work.This work was

supported by the National Natural Science Foundation of China (No. 21671128, 21671130).

Appendix A. Supporting Information

Figures showing: (S1) (a) Digital photograph of the complete sensor; (b) schematic diagram for the structure of gas sensor device. (S2) Digital photograph of the gas sensor test system. (S3) XRD pattern of Co-MOF. (S4) (a)TG and DTA analysis curves of the Co-MOF precursor; (b) TG analysis curves of Co_3O_4-300, Co_3O_4-400 and Co_3O_4-500; (S5) Nitrogen adsorption-desorption isotherms and BJH pore size distribution plots (inset) of (a)Co_3O_4-300, (b)Co_3O_4-400, (c)Co_3O_4-500.

References:

[1] M. Wang, Z. Shen, X. Zhao, F. Duanmu, H. Yu, H. Ji, Rational shape control of porous Co_3O_4 assemblies derived from MOF and their structural effects on n-butanol sensing, Journal of hazardous materials, 371 (2019) 352-361.

[2] A. Mirzaei, S.G. Leonardi, G. Neri, Detection of hazardous volatile organic compounds (VOCs) by metal oxide nanostructures-based gas sensors: A review, Ceramics International, 42 (2016) 15119-15141.

[3] M. Wang, T. Hou, Z. Shen, X. Zhao, H. Ji, MOF-derived Fe_2O_3: Phase control and effects of phase composition on gas sensing performance, Sensors and Actuators B: Chemical, 292 (2019) 171-179.

[4] M. Wang, T. Hou, X. Zhao, H. Yu, H. Ji, Crucial structural effects of porous Co_3O_4 derived from Prussian blue analogue on the enhanced gas sensing performance, Materials Letters, 242 (2019) 83-86.

[5] D. Zhang, Z. Yang, Z. Wu, G. Dong, Metal-organic frameworks-derived hollow zinc oxide/cobalt oxide nanoheterostructure for highly sensitive acetone sensing, Sensors and Actuators B: Chemical, 283 (2019) 42-51.

[6] F. Qu, T. Thomas, B. Zhang, X. Zhou, S. Zhang, S. Ruan, M. Yang, Self-sacrificing templated formation of $Co_3O_4/ZnCo_2O_4$ composite hollow nanostructures for highly sensitive detecting acetone vapor, Sensors and Actuators B: Chemical, 273 (2018) 1202-1210.

[7] T. Zou, R. Zhao, Z. Wang, R. Zhao, Z. Wang, Y. Yang, X. Xing, Y. Wang, Sensitive and selective n-butanol gas detection based on ZnO nanocrystalline synthesized by a low-temperature solvothermal method, Physica E: Low-dimensional Systems and Nanostructures, 103 (2018) 143-150.

[8] Y. Wang, Y. Zeng, L. Wang, Z. Lou, L. Qiao, H. Tian, W. Zheng, Ultrathin nanorod-assembled SnO_2 hollow cubes for high sensitive n-butanol detection, Sensors and Actuators B: Chemical, 283 (2019) 693-704.

[9] R. Zhao, Z. Wang, Y. Yang, X. Xing, T. Zou, Z. Wang, Y. Wang, Raspberry-like SnO_2 hollow nanostructure as a high response sensing material of gas sensor toward n-butanol gas, Journal of Physics and Chemistry of Solids, 120 (2018) 173-182.

[10] J. Wang, Z. Zheng, D. An, X. Tong, Q. Zhou, Highly selective n-butanol gas sensor based on porous In_2O_3 nanoparticles prepared by solvothermal treatment, Materials Science in Semiconductor Processing, 83 (2018) 139-143.

[11] Y. Wang, B. Zhang, J. Liu, Q. Yang, X. Cui, Y. Gao, X. Chuai, F. Liu, P. Sun, X. Liang, Y. Sun, G. Lu, Au-loaded mesoporous WO_3 : Preparation and n-butanol sensing performances, Sensors and Actuators B: Chemical, 236 (2016) 67-76.

[12] D. Han, Y. Ji, F. Gu, Z. Wang, Cobalt oxide nanorods with special pore structure for enhanced ethanol sensing performance, Journal of colloid and interface science, 531 (2018) 320-330.

[13] B. Zhang, X. Zhou, C. Jiang, F. Qu, M. Yang, Facile synthesis of mesoporous Co_3O_4 nanofans as gas sensing materials for selective detection of xylene vapor,

Materials Letters, 218 (2018) 127-130.

[14] X. Zhang, J. Wang, L. Xuan, Z. Zhu, Q. Pan, K. Shi, G. Zhang, Novel Co_3O_4 nanocrystalline chain material as a high performance gas sensor at room temperature, Journal of Alloys and Compounds, 768 (2018) 190-197.

[15] S. Mandal, M. Rakibuddin, R. Ananthakrishnan, Strategic synthesis of SiO2-modified porous Co_3O_4 nano-Octahedra through the nanocoordination polymer route for enhanced and selective sensing of H_2 Gas over NO_x, ACS omega, 3 (2018) 648-661.

[16] L. Li, M. Liu, S. He, W. Chen, Freestanding 3D mesoporous Co_3O_4@carbon foam nanostructures for ethanol gas sensing, Analytical chemistry, 86 (2014) 7996-8002.

[17] Y. Lu, W. Zhan, Y. He, Y. Wang, X. Kong, Q. Kuang, Z. Xie, L. Zheng, MOF-templated synthesis of porous Co_3O4 concave nanocubes with high specific surface area and their gas sensing properties, ACS applied materials & interfaces, 6 (2014) 4186-4195.

[18] T. Zhou, T. Zhang, J. Deng, R. Zhang, Z. Lou, L. Wang, P-type Co_3O_4 nanomaterials-based gas sensor: Preparation and acetone sensing performance, Sensors and Actuators B: Chemical, 242 (2017) 369-377

[19] X. Dong, Y. Su, T. Lu, L. Zhang, L. Wu, Y. Lv, MOFs-derived dodecahedra porous Co_3O_4: An efficient cataluminescence sensing material for H_2S, Sensors and Actuators B: Chemical, 258 (2018) 349-357.

[20] Y.M. Jo, T.H. Kim, C.S. Lee, K. Lim, C.W. Na, F. Abdel-Hady, A.A. Wazzan, J.H. Lee, Metal-organic framework-derived hollow hierarchical Co_3O_4 nanocages with tunable size and morphology: ultrasensitive and highly selective detection of methylbenzenes, ACS applied materials & interfaces, 10 (2018) 8860-8868.

[21] K.I. Choi, H.R. Kim, K.M. Kim, D. Liu, G. Cao, J.H. Lee, C_2H_5OH sensing characteristics of various Co_3O_4 nanostructures prepared by solvothermal reaction, Sens. Actuators, B, 146 (2010) 183-189.

[22] J. Tan, M. Dun, L. Li, X. Huang, Co_3O_4 nanoboxes with abundant porestructure boosted ultrasensitive toluene gas sensors, Materials Research Express, 5 (2018) 045036.

[23] Z. Wen, L. Zhu, W. Mei, L. Hu, X. Li, L. Sun, H. Cai, Z. Ye, Rhombus-shaped Co_3O_4 nanorod arrays for high-performance gas sensor, Sens. Actuators, B, 186 (2013) 172-179.

[24] R. Jiang, L. Jia, X. Guo, Z. Zhao, J. Du, X. Wang, P. Wang, F. Xing, Dimethyl sulfoxide-assisted hydrothermal synthesis of Co_3O_4-based nanorods for selective and sensitive diethyl ether sensing, Sensors and Actuators B: Chemical, 290 (2019) 275-284.

[25] L. Guo, F. Chen, N. Xie, C. Wang, X. Kou, Y. Sun, J. Ma, X. Liang, Y. Gao, G. Lu, Metal-organic frameworks derived tin-doped cobalt oxide yolk-shell nanostructures and their gas sensing properties, Journal of colloid and interface science, 528 (2018) 53-62.

[26] J. Wu, Y. Yang, C. Zhang, H. Yu, L. Huang, X. Dong, J. Wang, X. Wang, Extremely sensitive and accurate H_2S sensor at room temperature fabricated with In-doped Co_3O_4 porous nanosheets, Dalton transactions, 48 (2019) 7720-7727.

[27] W.T. Koo, S. Yu, S.J. Choi, J.S. Jang, J.Y. Cheong, I.D. Kim, Nanoscale PdO Catalyst Functionalized Co3O4 Hollow Nanocages Using MOF Templates for Selective Detection of Acetone Molecules in Exhaled Breath, ACS applied materials & interfaces, 9 (2017) 8201-8210.

[28] S.J. Hwang, K.I. Choi, J.W. Yoon, Y.C. Kang, J.H. Lee, Pure and palladium-loaded Co_3O_4 hollow hierarchical nanostructures with giant and ultraselective chemiresistivity to xylene and toluene, Chemistry, 21 (2015) 5872-5878.

[29] J. Xiao, K. Diao, Z. Zheng, X. Cui, MOF-derived porous ZnO/Co_3O_4 nanocomposites for high performance acetone gas sensing, Journal of Materials Science: Materials in Electronics, 29 (2018) 8535-8546.

[30] S. Shi, F. Zhang, H. Lin, Q. Wang, E. Shi, F. Qu, Enhanced triethylamine-sensing properties of P-N heterojunction Co_3O_4/In_2O_3 hollow microtubes derived from metal–organic frameworks, Sensors and Actuators B: Chemical, 262 (2018) 739-749.

[31] B. Li, J. Liu, Q. Liu, R. Chen, H. Zhang, J. Yu, D. Song, J. Li, M. Zhang, J. Wang, Core-shell structure of ZnO/Co_3O_4 composites derived from bimetallic-organic frameworks with superior sensing performance for ethanol gas, Applied Surface Science, 475 (2019) 700-709.

[32] S. Gao, Y. Sui, F. Wei, J. Qi, Q. Meng, Y. Ren, Y. He, Dandelion-like nickel/cobalt metal-organic framework based electrode materials for high performance supercapacitors, Journal of colloid and interface science, 531 (2018) 83-90.

[33] M.A. Ahsan, V. Jabbari, M.T. Islam, R.S. Turley, N. Dominguez, H. Kim, E. Castro, J.A. Hernandez-Viezcas, M.L. Curry, J. Lopez, J.L. Gardea-Torresdey, J.C. Noveron, Sustainable synthesis and remarkable adsorption capacity of MOF/graphene oxide and MOF/CNT based hybrid nanocomposites for the removal of Bisphenol A from water, The Science of the total environment, 673 (2019) 306-317.

[34] S. Rezaee, S. Shahrokhian, Facile synthesis of petal-like NiCo/NiO-CoO/nanoporous carbon composite based on mixed-metallic MOFs and their application for electrocatalytic oxidation of methanol, Applied Catalysis B: Environmental, 244 (2019) 802-813.

[35] P. Horcajada, T. Chalati, C. Serre, B. Gillet, C. Sebrie, T. Baati, J.F. Eubank, D. Heurtaux, P. Clayette, C. Kreuz, J.S. Chang, Y.K. Hwang, V. Marsaud, P.N. Bories, L. Cynober, S. Gil, G. Ferey, P. Couvreur, R. Gref, Porous metal-organic-framework nanoscale carriers as a potential platform for drug delivery and imaging, Nature materials, 9 (2010) 172-178.

[36] R. Zhang, T. Zhou, L. Wang, T. Zhang, Metal-organic frameworks-derived hierarchical Co_3O_4 Structures as efficient sensing materials for acetone detection, ACS applied materials & interfaces, 10 (2018) 9765-9773.

[37] Y. Xiong, W. Xu, Z. Zhu, Q. Xue, W. Lu, D. Ding, L. Zhu, ZIF-derived porous ZnO-Co_3O_4 hollow polyhedrons heterostructure with highly enhanced ethanol detection performance, Sensors and Actuators B: Chemical, 253 (2017) 523-532.

[38] Y. Wang, M. Kong, Z. Liu, C. Lin, Y. Zeng, Morella-rubra-like metal–organic-framework-derived multilayered Co_3O_4/NiO/C hybrids as high-performance anodes for lithium storage, Journal of Materials Chemistry A, 5 (2017) 24269-24274.

[39] J. Deng, R. Zhang, L. Wang, Z. Lou, T. Zhang, Enhanced sensing performance of the Co_3O_4 hierarchical nanorods to NH_3 gas, Sensors and Actuators B: Chemical, 209 (2015) 449-455.

[40] I. Lee, S. Choi, H.J. Lee, M. Oh, Hollow Metal–organic framework microparticles assembled via a self-templated formation mechanism, Crystal Growth & Design, 15 (2015) 5169-5173.

[41] X. Liu, F. Zou, K. Liu, Z. Qiang, C.J. Taubert, P. Ustriyana, B.D. Vogt, Y. Zhu, A binary metal organic framework derived hierarchical hollow Ni_3S_2/Co_9S_8/N-doped carbon composite with superior sodium storage performance, Journal of Materials Chemistry A, 5 (2017) 11781-11787.

[42] H.-S. Lu, H. Zhang, X. Zhang, N. Sun, X. Zhu, H. Zhao, G. Wang, Transformation of carbon-encapsulated metallic Co into ultrafine Co/CoO nanoparticles exposed on N-doped graphitic carbon for high-performance rechargeable zinc-air battery, Applied Surface Science, 448 (2018) 369-379.

[43] T. Meng, Q.-Q. Xu, Z.-H. Wang, Y.-T. Li, Z.-M. Gao, X.-Y. Xing, T.-Z. Ren, Co_3O_4 nanorods with self-assembled nanoparticles in queue for supercapacitor, Electrochimica Acta, 180 (2015) 104-111.

[44] D. Ge, J. Peng, G. Qu, H. Geng, Y. Deng, J. Wu, X. Cao, J. Zheng, H. Gu, Nanostructured Co(ii)-based MOFs as promising anodes for advanced lithium storage, New Journal of Chemistry, 40 (2016) 9238-9244.

[45] J. Zhang, H. Lu, L. Zhang, D. Leng, Y. Zhang, W. Wang, Y. Gao, H. Lu, J. Gao, G. Zhu, Z. Yang, C. Wang, Metal–organic framework-derived ZnO hollow nanocages functionalized with nanoscale Ag catalysts for enhanced ethanol sensing properties, Sensors and Actuators B: Chemical, 291 (2019) 458-469.

[46] J. Hu, C. Zou, Y. Su, M. Li, Z. Yang, M. Ge, Y. Zhang, One-step synthesis of 2D C_3N_4-tin oxide gas sensors for enhanced acetone vapor detection, Sensors and Actuators B: Chemical, 253 (2017) 641-651.

[47] J. Cao, S. Wang, H. Zhang, T. Zhang, Constructing one dimensional Co_3O_4 hierarchical nanofibers as efficient sensing materials for rapid acetone gas detection, Journal of Alloys and Compounds, 799 (2019) 513-520.

[48] C. Su, L. Zhang, Y. Han, X. Chen, S. Wang, M. Zeng, N. Hu, Y. Su, Z. Zhou, H. Wei, Z. Yang, Glucose-assisted synthesis of hierarchical flower-like Co_3O_4 nanostructures assembled by porous nanosheets for enhanced acetone sensing, Sensors and Actuators B: Chemical, 288 (2019) 699-706.

[49] Y. Lin, H. Ji, Z. Shen, Q. Jia, D. Wang, Enhanced acetone sensing properties of

Co3O4 nanosheets with highly exposed (111) planes, Journal of Materials Science: Materials in Electronics, 27 (2015) 2086-2095.

[50] W. Zhou, Y.P. Wu, J. Zhao, W.W. Dong, X.Q. Qiao, D.F. Hou, X. Bu, D.S. Li, Efficient gas-sensing for formaldehyde with 3D hierarchical Co_3O_4 derived from Co_5-based MOF microcrystals, Inorganic chemistry, 56 (2017) 14111-14117.

[51] Z. Jin, L.-P. Wang, Y. Zhang, J. Fan, M.-H. Liao, X.-F. Wang, Y. Ding, Highly sensitive and selective ethanol sensors based on porous Co_3O_4 nanobelts synthesized through a facile wet-chemistry method, Journal of Nanoparticle Research, 21 (2019).

[52] L.L. Wang, J.A. Deng, Z. Lou, T. Zhang, Nanoparticles-assembled Co_3O_4 nanorods p-type nanomaterials: One-pot synthesis and toluene-sensing properties, Sens. Actuator B-Chem., 201 (2014) 1-6.

[53] T. Li, Z. Shen, Y. Shu, X. Li, C. Jiang, W. Chen, Facet-dependent evolution of surface defects in anatase TiO_2 by thermal treatment: implications for environmental applications of photocatalysis, Environmental Science: Nano, 6 (2019) 1740-1753.

[54] J.M. Xu, J.P. Cheng, The advances of Co_3O_4 as gas sensing materials: A review, Journal of Alloys and Compounds, 686 (2016) 753-768.

[55] J. Guo, Y. Li, B. Jiang, H. Gao, G. Hao, Xylene gas sensing properties of hydrothermal synthesized SnO_2-Co_3O_4 microstructure, Sensors and Actuators B: Chemical, 310 (2020) 127780.

[56] Z. Zhang, L. Zhu, Z. Wen, Z. Ye, Controllable synthesis of Co_3O_4 crossed

nanosheet arrays toward an acetone gas sensor, Sensors and Actuators B: Chemical, 238 (2017) 1052-1059.

Figure captions

Scheme. 1. Schematic illustration for the preparation process of Co_3O_4 nanospheres with different structures.

Fig. 1. XRD patterns of Co_3O_4 nanospheres at different calcination temperatures.

Fig. 2. FESEM images of (a, b) Co-MOF nanospheres; and Co_3O_4 products of (c, d) Co_3O_4-300; (e, f) Co_3O_4-400; (g, h) Co_3O_4-500.

Fig. 3. TEM images of (a) Co_3O_4-300; (b) Co_3O_4-400; (c) Co_3O_4-500; (d) HRTEM images of Co_3O_4-400, inset is the SAED image of Co_3O_4-400.

Fig. 4. Response of Co_3O_4 sensors to 100 ppm n-butanol at different temperatures.

Fig. 5. (a)Transient response curve of Co_3O_4 sensors; Response and recovery curves of (b) Co_3O_4-300, (c) Co_3O_4-400, (d) Co_3O_4-500 sensors to 100 ppm n-butanol at the optimal operating temperature.

Fig. 6. (a) sensing transient curves to different concentration of n-butanol at 140℃,the inset shows the enlarged dynamic sensing curves at n-butanol concentrations of 3 and 5ppm ; (b)Response of Co_3O_4 samples to different ethanol concentrations;(c) The corresponding relationship between response and concentration;(d) Six periods of response–recovery curves to 100 ppm n-butanol at 140℃;(e) Responses of Co_3O_4 samples to different gases at 140℃;(f) Long-term stability of the Co_3O_4-400 based gas sensor.

Fig. 7. (a) XPS spectra of Co 2p for porous Co_3O_4 samples; XPS spectra of O 1s and curve-fitting for (b) Co_3O_4-300, (c) Co_3O_4-400, (d) Co_3O_4-500.

Fig. 8. The schematic diagram for gas sensing mechanism of the Co_3O_4 nanospheres based sensor.

Table1. Comparison of varied nanostructured Co_3O_4 in VOCs sensing performances.

Scheme 1.

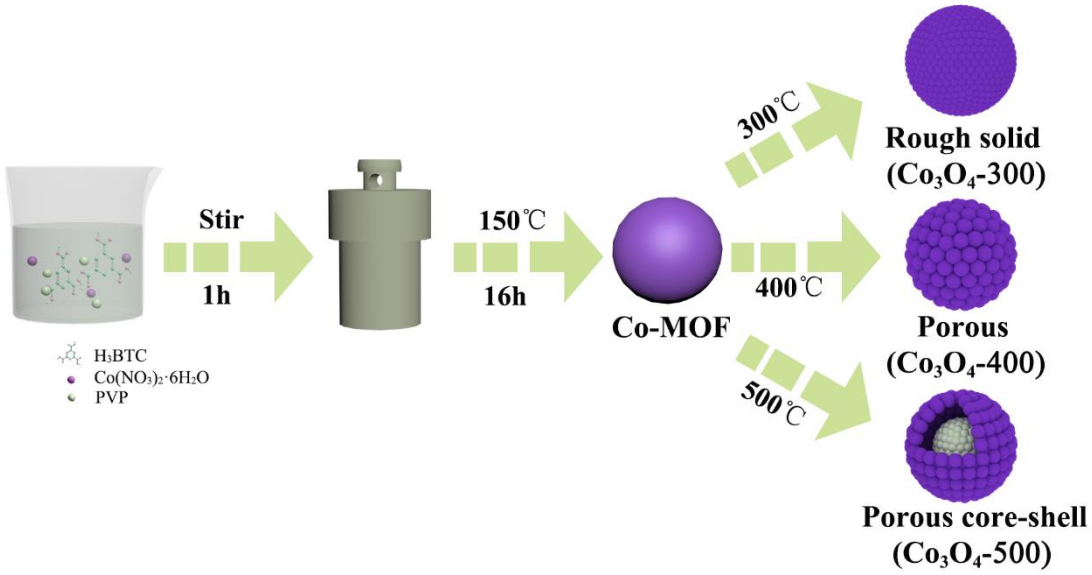
Stir
1h
150℃
16h
Co-MOF
300℃
Rough solid
(Co3O4-300)
400℃
Porous
(Co3O4-400)
500℃
Porous core-shell
(Co3O4-500)
H3BTC
Co(NO3)2·6H2O
PVP

Fig. 1.

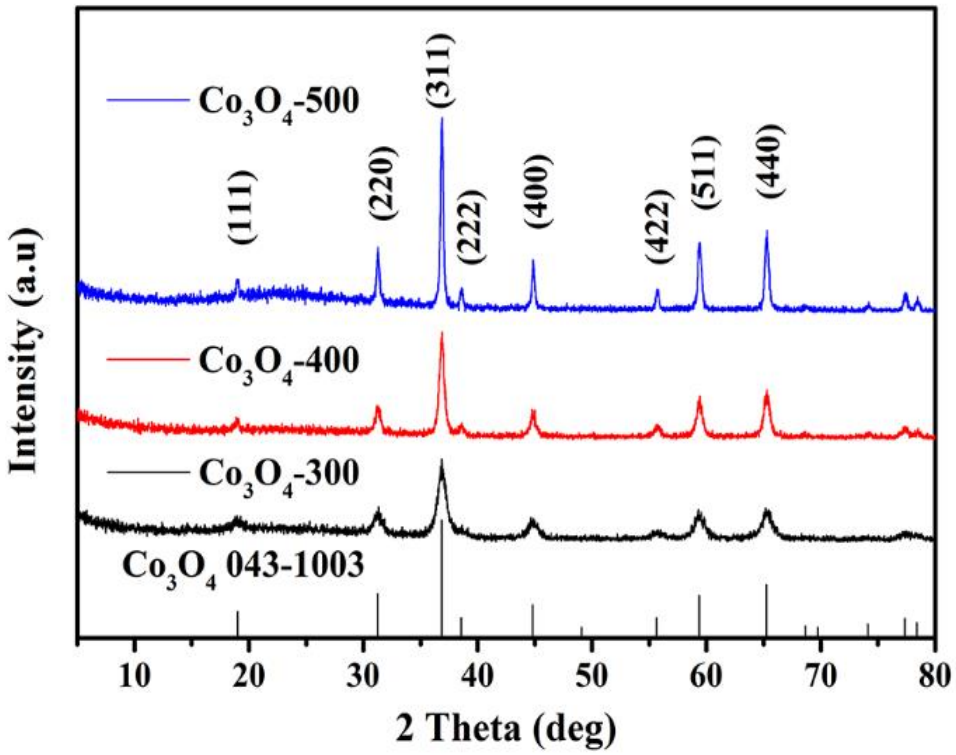
Co3O4-500
(111)
(220)
(311)
(222)
(400)
(422)
(511)
(440)
Co3O4-400
Co3O4-300
Co3O4 043-1003
Intensity (a.u)
10
20
30
40
50
60
70
80
2 Theta (deg)

Fig. 2.

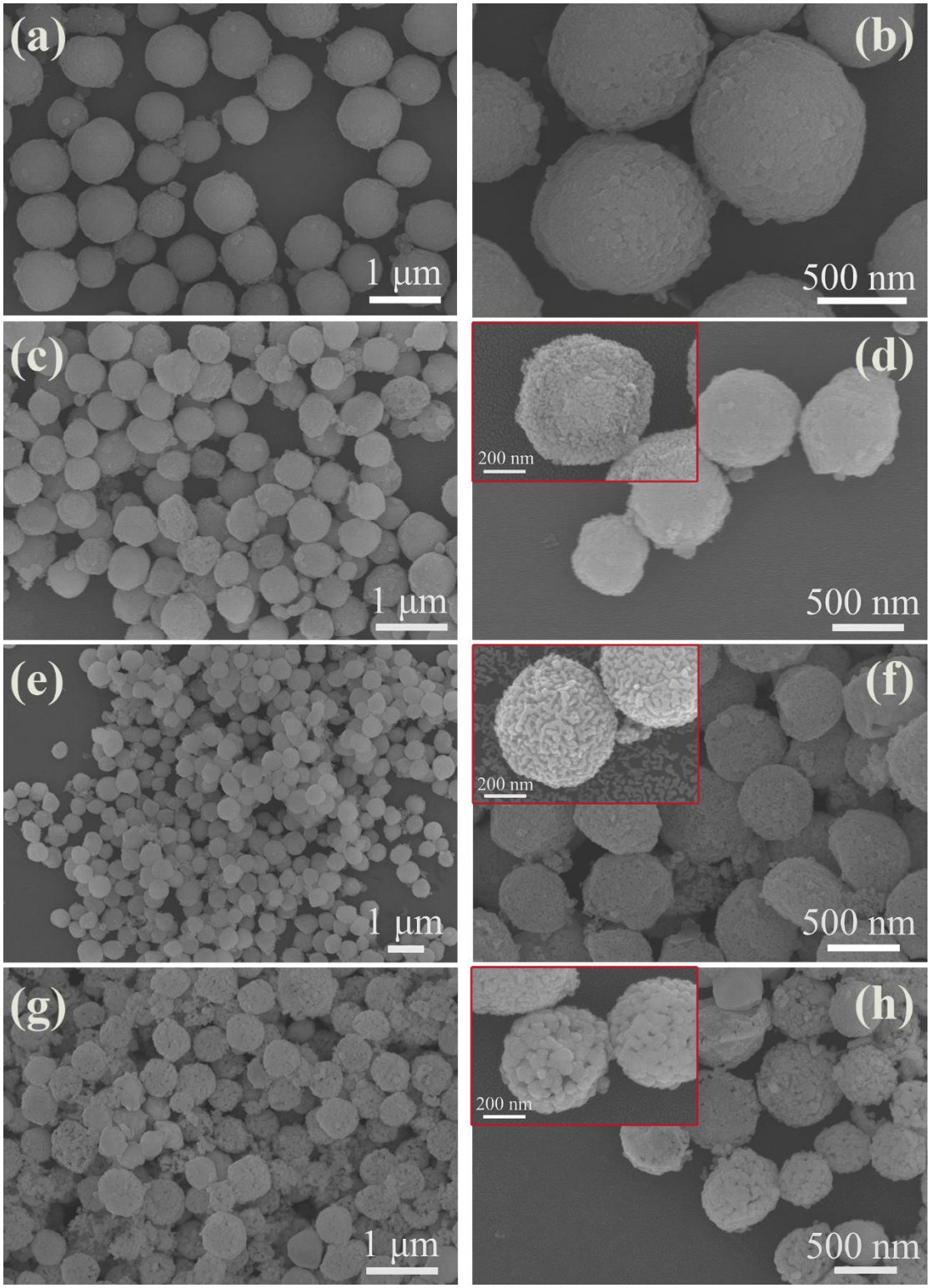
(a)
1 μm
(b)
500 nm
(c)
1 μm
(d)
200 nm
500 nm
(e)
1 μm
(f)
200 nm
500 nm
(g)
1 μm
(h)
200 nm
500 nm

Fig. 3.

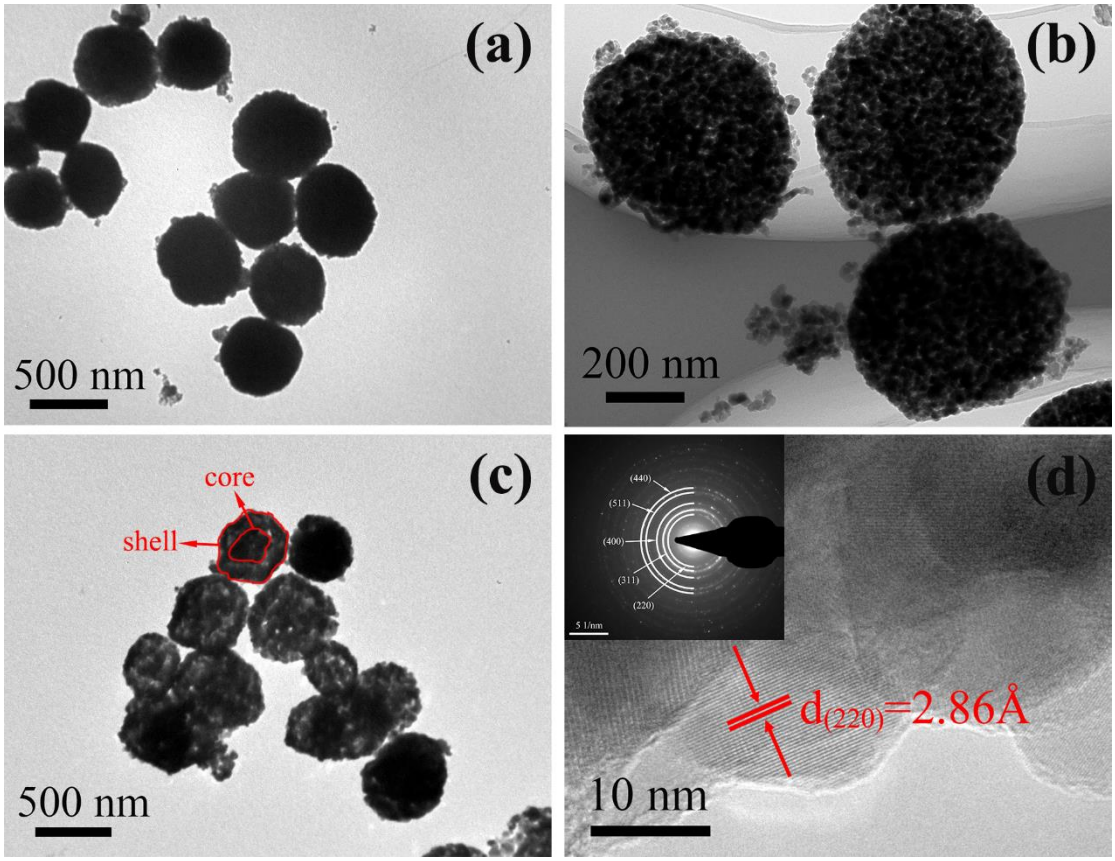
(a)
500 nm
(b)
200 nm
(c)
core
shell
500 nm
(d)
(440)
(511)
(400)
(311)
(220)
5 1/nm
d(220)=2.86Å
10 nm

Fig. 4.

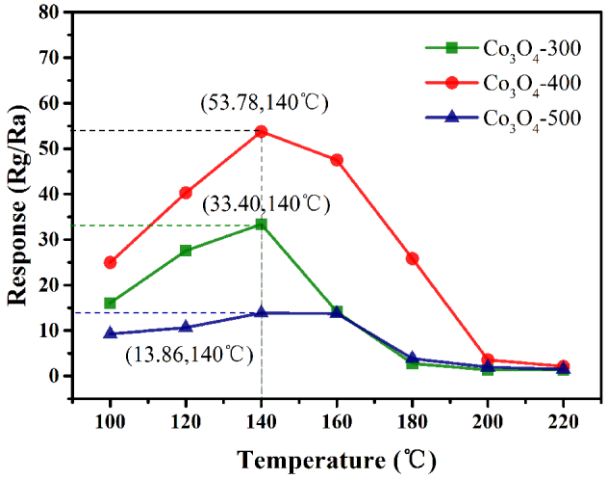
Response (Rg/Ra)
Temperature (℃)
Co3O4-300
Co3O4-400
Co3O4-500
(53.78,140℃)
(33.40,140℃)
(13.86,140℃)
0
10
20
30
40
50
60
70
80
100
120
140
160
180
200
220

Fig. 5.

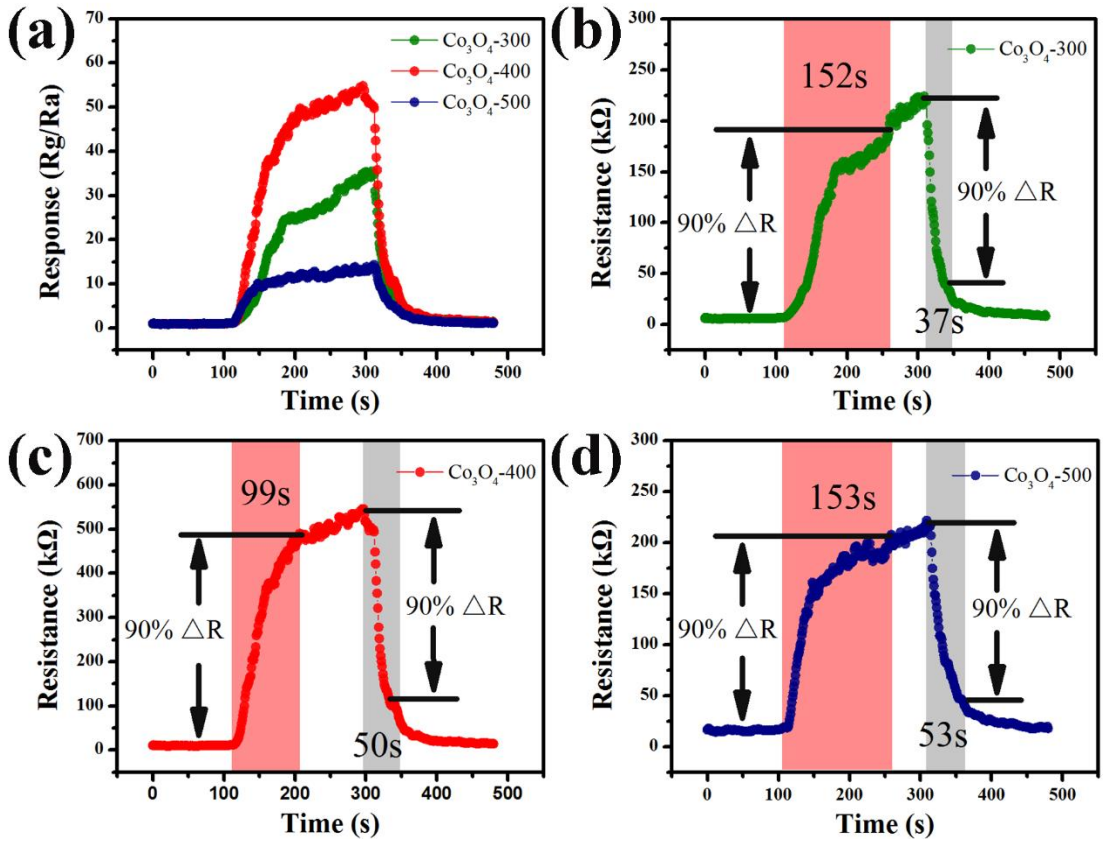
(a)
Response (Rg/Ra)
Time (s)
Co3O4-300
Co3O4-400
Co3O4-500
(b)
Resistance (kΩ)
Time (s)
152s
37s
90% △R
90% △R
Co3O4-300
(c)
Resistance (kΩ)
Time (s)
99s
50s
90% △R
90% △R
Co3O4-400
(d)
Resistance (kΩ)
Time (s)
153s
53s
90% △R
90% △R
Co3O4-500

Fig. 6.

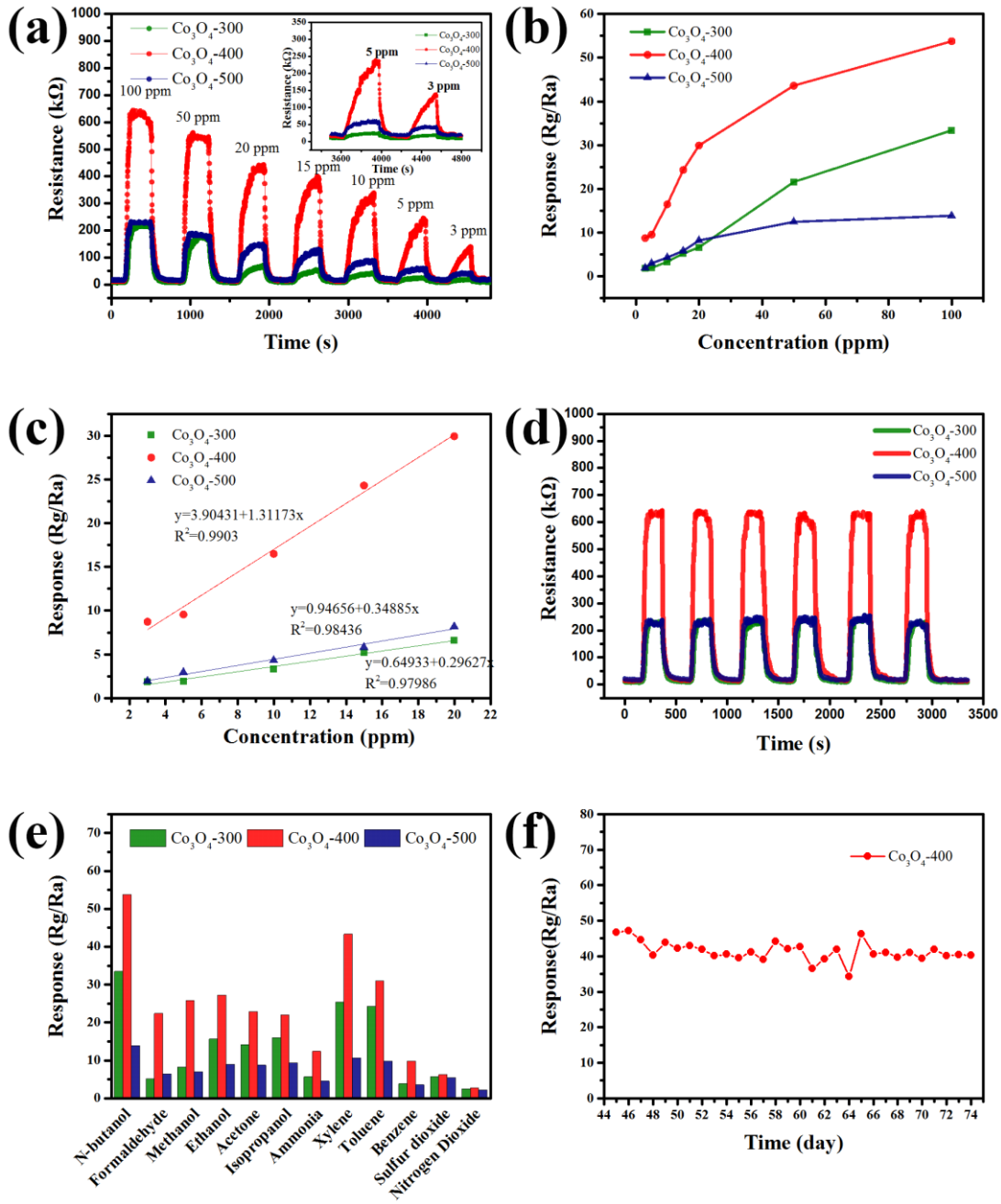
(a)
Co3O4-300
Co3O4-400
Co3O4-500
100 ppm
50 ppm
20 ppm
15 ppm
10 ppm
5 ppm
3 ppm
Resistance (kΩ)
Time (s)
(b)
Response (Rg/Ra)
Concentration (ppm)
(c)
y=3.90431+1.31173x
R2=0.9903
y=0.94656+0.34885x
R2=0.98436
y=0.64933+0.29627x
R2=0.97986
(d)
(e)
N-butanol
Formaldehyde
Methanol
Ethanol
Acetone
Isopropanol
Ammonia
Xylene
Toluene
Benzene
Sulfur dioxide
Nitrogen Dioxide
(f)
Response(Rg/Ra)
Time (day)

Fig. 7.

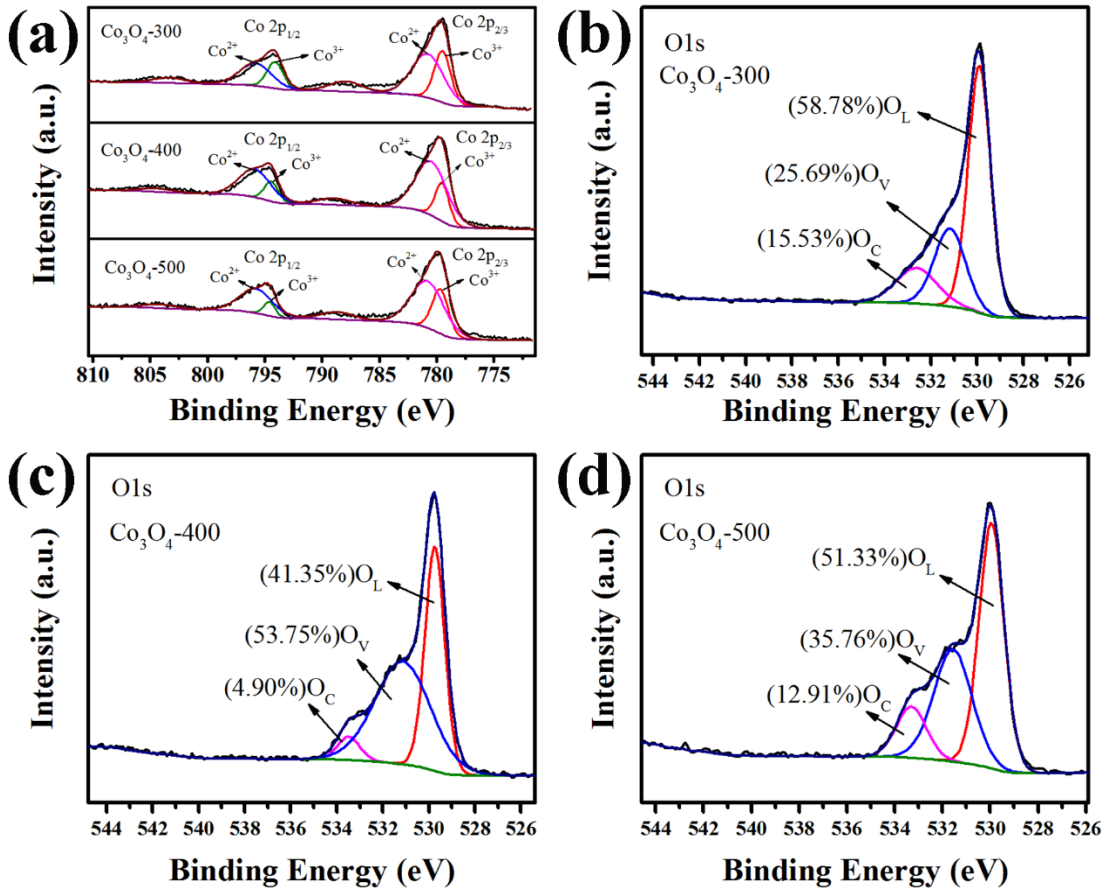
(a)
Co3O4-300
Co 2p1/2
Co2+
Co3+
Co 2p2/3
Co2+
Co3+
Co3O4-400
Co 2p1/2
Co2+
Co3+
Co 2p2/3
Co2+
Co3+
Co3O4-500
Co 2p1/2
Co2+
Co3+
Co 2p2/3
Co2+
Co3+
Intensity (a.u.)
810 805 800 795 790 785 780 775
Binding Energy (eV)
(b)
O1s
Co3O4-300
(58.78%)OL
(25.69%)OV
(15.53%)OC
Intensity (a.u.)
544 542 540 538 536 534 532 530 528 526
Binding Energy (eV)
(c)
O1s
Co3O4-400
(41.35%)OL
(53.75%)OV
(4.90%)OC
Intensity (a.u.)
544 542 540 538 536 534 532 530 528 526
Binding Energy (eV)
(d)
O1s
Co3O4-500
(51.33%)OL
(35.76%)OV
(12.91%)OC
Intensity (a.u.)
544 542 540 538 536 534 532 530 528 526
Binding Energy (eV)

Fig. 8.

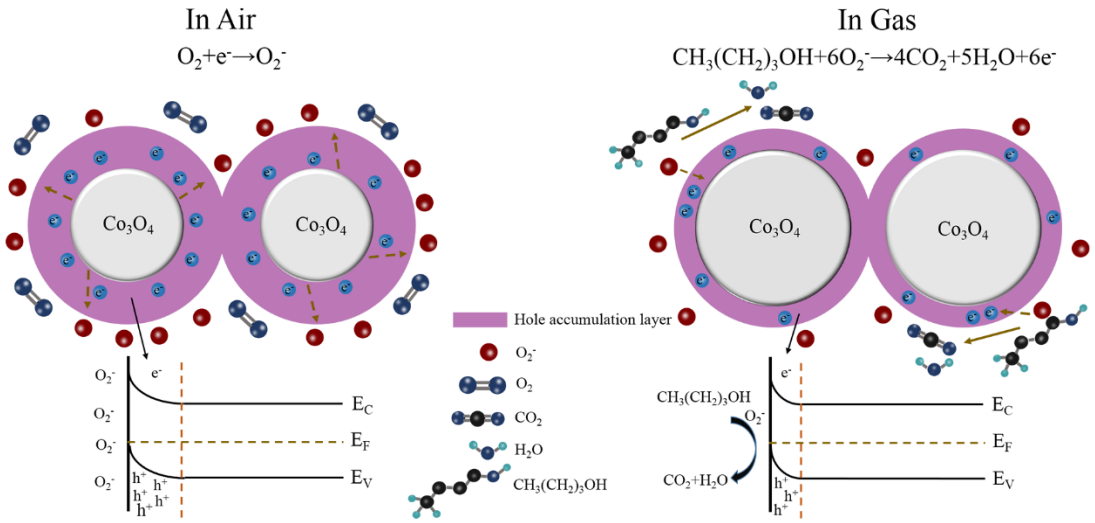
In Air
$O_2+e^-\rightarrow O_2^-$
In Gas
$CH_3(CH_2)_3OH+6O_2^-\rightarrow 4CO_2+5H_2O+6e^-$
Co_3O_4
Co_3O_4
Co_3O_4
Co_3O_4
Hole accumulation layer
O_2^-
O_2
CO_2
H_2O
$CH_3(CH_2)_3OH$
E_C
E_F
E_V
$CH_3(CH_2)_3OH$
CO_2+H_2O

Table1.

Materials	gas	Concentration (ppm)	Response (Rg/Ra)	Working temperature (℃)	Response/ Recovery time (s)	Ref.
Co_3O_4 hierarchical nanofibers	acetone	100	9.3	190	7/1	[47]
hierarchical flower-like Co_3O_4 nanostructures	acetone	100	48.1	130	18/13	[48]
Co_3O_4 nanosheets	acetone	100	6.1	160	98/7	[49]
3D Hierarchical Co_3O_4 spheres	formaldehyde	100	12	170	46/98	[50]
porous Co_3O_4 nanobelts	ethanol	100	20.3	300	15/20	[51]
Co_3O_4 nanorods	toluene	200	35	200	90/55	[52]
porous Co_3O_4 octadecahedron	n-butanol	100	21	100	146/90	[1]
porous Co_3O_4 nanospheres	**n-butanol**	**100**	**53.78**	**140**	**99/50**	**This work**

*Declaration of Interest Statement

Declaration of interests

☒ The authors declare that they have no known competing financial interests or personal relationships that could have appeared to influence the work reported in this paper.

☐The authors declare the following financial interests/personal relationships which may be considered as potential competing interests: